Interactions of magnetohydrodynamic waves with gravitomagnetic fields, and their possible roles in black-hole magnetospheres

Xiao-He Zhang
Theoretical Astrophysics 130-33, California Institute of Technology, Pasadena, California 91125
(Received 19 July 1989)

The magnetospheres of rotating, magnetized black holes are thought to generate some of the jets observed in quasars and active galactic nuclei. Previous research on such magnetospheres has focused on stationary configurations. This paper is an initial, exploratory study of dynamical magnetospheres. Because a dynamical study in a rotating hole's Kerr spacetime would be exceedingly difficult, this paper introduces a class of simpler, plane-symmetric or cylindrically symmetric model spacetimes in which to explore the dynamics. These model spacetimes preserve the key physical features of the Kerr geometry: they have a Kerr-type gravitomagnetic potential (shift function), a Kerr-type horizon, and a Kerr-type asymptotically flat region far from the horizon. This first exploratory study is restricted to the simplest of these spacetimes, one with the planar metric $ds^2=-dt^2+(dx+\beta\,dt)^2+dy^2+dz^2$, gravitomagnetic potential $\beta=V_F(\tanh z-1)$, and horizon lateral velocity $dx/dt=2V_F$. In this spacetime the asymptotically flat region is at $z\gg 1$, and the horizon has been pushed off to $z=-\infty$. We treat the dynamical magnetospheres using the 3+1 formalism of general-relativistic magnetohydrodynamics (GRMHD) developed in an earlier paper. Kerr-type models of stationary magnetospheres are built in this spacetime as exact solutions to the fully nonlinear equations of GRMHD. In these solutions the magnetic field, under the influence of the horizon's lateral motion, is driven to move laterally with velocity $dx/dt=V_F$; and plasma particles (e^+e^- pairs) are created at $z=0$, and are then driven up to relativistic velocities by magnetic-gravitomagnetic coupling, as they flow off to "infinity" ($z=+\infty$) and down toward the "horizon" ($z=-\infty$). Weak perturbations of these analytic magnetospheres are studied using a linearization of the GRMHD perturbation equations. The linearized perturbation equations are Fourier analyzed in t and x [$\exp(-i\omega t+ik_x x)$] and are solved numerically to obtain the z dependence of the perturbations. The numerical solutions describe the response of the magnetosphere to oscillatory driving forces in the plasma-injection plane, $z=0$. This models the response of a Kerr hole's magnetosphere to oscillatory driving forces near the plasma-production region—forces that might arise when lumpy magnetic fields, anchored in an accretion disk, orbit the hole, pressing inward on the magnetosphere. In our model spacetime the magnetosphere responds resonantly at frequencies (as measured at infinity) $\omega=k_x V_F$, i.e., at frequencies for which the perturbations are stationary as seen in the field lines' rest frame. The analog for a Kerr magnetosphere would be resonant responses at $\omega=m\Omega_F$, where m is the azimuthal quantum number of the perturbation and Ω_F is the field-line angular velocity (roughly equal to half the horizon angular velocity). Such resonances, if they occur in real black-hole magnetospheres, would show up as a modulation of the jet's outflowing energy flux.

I. INTRODUCTION

In recent decades, the huge energy output (up to $\sim 10^{48}$ ergs/sec) from active galactic nuclei (AGN's) has been firmly established, and theories using a supermassive central black hole ($\sim 10^8 M_\odot$) to explain this energy output have been developed and become well accepted.[1] There are also some recent observations that suggest the existence of supermassive black holes at the centers of some nearby galaxies.[2]

One of the most attractive models for powering jets in AGN's is electrodynamical [or magnetohydrodynamic (MHD)] extraction of the rotational energy of a magnetized, supermassive black hole,[3–5] the "Blandford-Znajek effect." In this model the hole is threaded by a magnetic field, which is held on it by the Maxwell pressure of surrounding fields that are anchored in an accretion disk. (If the disk were suddenly removed, the field threading the hole would fly away.) The rotation of the hole (as embodied in the hole's "gravitomagnetic potential" or "shift function" β) interacts with the threading magnetic field **B** to produce an intense electric field **E**, which in turn accelerates charged particles to high speeds, causing them to radiate or Compton scatter. The resulting high-energy photons then interact with the charged particles or the **B** field to produce a rich plasma of electron-positron pairs.[6–8] In this way, the hole's magnetosphere is kept filled with plasma. The plasma is created near the hole (at something like two black-hole radii). The rotation of the hole and its magnetic field lines (i.e., the "gravitomagnetic-magnetic coupling"), then drives some of the plasma to flow into the horizon and some off toward infinity, forming an MHD wind, which becomes the observed jet when far from the hole.

All previous studies of this model have focused on stationary, steady-state magnetospheres. This has been justified by the fact that the hole's horizon "cleans" the field lines that thread it,[4,9] leaving them (approximately) smooth and axisymmetric. More specifically, the horizon-threading **B** field was originally, long ago, embedded in the accretion disk. Differential rotation of the disk amplified the field and then reconnection made it tangled and chaotic. This chaotic field was then carried onto the horizon by the disk's accreting plasma, and the horizon then quickly "cleaned" the field; i.e., it got rid of all closed loops and helped the remaining field to distribute itself in a smooth, approximately axisymmetric way, over the horizon.

Despite this cleaning process, the hole's **B** field should not be precisely axisymmetric. Nonaxisymmetric perturbations will be produced by the external agent that holds the field on the hole—the chaotic, disk-anchored **B** field that presses in on the smoother, hole-threading field. As lumps of disk-anchored field orbit the hole, their Maxwell pressure will buffet the hole-threading field, thereby creating (near the plasma-production region) oscillatory perturbations of the magnetosphere. These perturbations presumably will give rise to MHD waves, some of which propagate into the horizon and others off toward infinity, along with the accelerated plasma. The result should be an oscillatory modulation of the energy carried by the magnetosphere's wind and jet.

This scenario for nonaxisymmetric effects in a black-hole magnetosphere is totally speculative, since nobody has yet attempted an analysis of dynamical, nonaxisymmetric perturbations. The purpose of this paper is to carry out a first, exploratory analysis of such perturbations.

Even in the stationary, axisymmetric case, the modeling of a black-hole magnetosphere is very difficult: Blandford and Znajek[3] simplified their original analysis by focusing attention, primarily, on the near-horizon region, which they assumed to be force-free, axisymmetric, and stationary. Macdonald[10] succeeded in solving numerically the two-dimensional, partial-differential stream equation for the structure of the force-free region; but his analysis and that of Blandford and Znajek had to assume somewhat arbitrary boundary conditions at the outer edge of the force-free region, where plasma inertia begins to be important. In order to obtain an unified, global treatment of the entire stationary magnetosphere (the inner force-free region, the wind region, the jet region), Phinney[5] assumed that the plasma would everywhere be so highly conducting that perfect MHD describes it well; and then, with the aid of a clever analysis of the magnetosphere's boundary conditions (and avoiding the task of actually solving the MHD version of the stream equation), he was able to infer a variety of properties of the outflowing MHD wind and jet.

To solve the MHD stream equation in the Kerr spacetime of a rotating hole is so difficult that nobody has yet tackled it, so far as we know—except in the case of a nonrotating hole.[11,12] To solve for the dynamical behavior of a perturbed magnetosphere in the Kerr spacetime would be even more difficult.

The difficulties are so great that we have chosen a different route: We have altered the spacetime in which the magnetosphere lives so as to simplify the analysis. The main source of difficulty with the Kerr spacetime is its low symmetry: it is stationary (independent of time t) and axisymmetric (independent of angle ϕ); but that is all: it has nontrivial dependences on radius r and polar angle θ. To make the analysis tractable, we add one more symmetry—and demand that it be a symmetry not only of the spacetime, but also of the equilibrium magnetosphere—and we do so while preserving the key features of the Kerr metric: its horizon, its asymptotically flat distant region, and its gravitomagnetic potential. The resulting, altered spacetimes and their horizons are all cylindrical or planar; see Sec. II for full details.

These model spacetimes should be useful not only for getting insight into dynamical perturbations of a black-hole magnetosphere (the goal of this paper), but also for studying the details of how such a magnetosphere, when first formed, settles down into its equilibrium configuration. That settling down and the resulting equilibrium are a subject of current controversy: one issue is whether the equilibrium state will be that of Blandford and Znajek, which can extract the hole's rotational energy via electrodynamic process.[13,14]

In this paper we study magnetospheric dynamics in the simplest of the model spacetimes: one with the planar metric

$$ds^2=-dt^2+(dx+\beta\, dt)^2+dy^2+dz^2\ , \tag{1.1}$$

which has a gravitomagnetic potential (shift function) $\beta=\beta\partial/\partial x$ where

$$\beta=V_F(\tanh z-1)\ . \tag{1.2}$$

(We shall henceforth refer to the scalar field β as the shift function.) In this spacetime the asymptotically flat region is at $z\gg 1$, and the horizon has been pushed off to $z=-\infty$; i.e., it has been converted into a second asymptotically flat region. Our reason for getting rid of the horizon is our desire to study, as cleanly and simply as possible, the interaction of the gravitomagnetic potential β with the magnetosphere. We strongly suspect (but only future calculations will show for sure) that the horizon is rather unimportant: The key gravitational influences on the magnetosphere are all due to the the gravitomagnetic potential. The z direction in this spacetime is the analog of the radial r direction in Kerr; the x direction is the analog of Kerr's axial ϕ direction; the y direction is the analog of Kerr's poloidal θ direction; and t is the analog of the Kerr metric's time coordinate t. The Kerr metric depends nontrivially on both r and θ, whereas the metric (1.1) depends nontrivially on only z. In our model spacetime (1.1) the "horizon," $z=-\infty$, moves in the x direction with speed $dx/dt=2V_F$ relative to "infinity," $z=+\infty$. This is analogous to the rotational motion of a Kerr hole's horizon with angular velocity $d\phi/dt=\Omega_H$ relative to infinity, $r=+\infty$.

In Secs. III and IV we build models for stationary magnetospheres in this model spacetime. Our models are exact, analytic solutions to the general-relativistic magnetohydrodynamic (GRMHD) equations, with the plasma

assumed for simplicity to be "cold" (negligible particle pressure). The magnetosphere's magnetic field lines extend out of the "horizon" ($z=-\infty$) and off to "infinity" ($z=+\infty$). The plasma is created in the central plane $z=0$ [analog of the plasma creation region $r\sim 2$ (black-hole radii) in Kerr]; and some of the plasma then flows down to the "horizon," while the rest flows off to "infinity." The perfect conductivity of the flowing plasma, forces the field lines to move rigidly in the x direction with a velocity equal to half the horizon's velocity, $dx/dt=V_F$. The outflowing plasma is accelerated along the **B**-field lines by the joint action of the field-line motion and the gravitomagnetic potential—i.e., by "magnetic-gravitomagnetic coupling." The asymptotic velocity of the plasma as it approaches $z=\pm\infty$ is always less than or equal to the speed of fast magnetosonic waves.

In Secs. V and VI we analyze weak, linearized perturbations of our stationary magnetospheric models—with the perturbations confined, for simplicity, to the x-z plane (no dependence on y). Section V derives a set of linearized GRMHD equations for the perturbations [Eqs. (5.6)] and a set of junction conditions at the $z=0$ (plasma production) plane [Eqs. (5.7)]. These two sets of equations are then Fourier analyzed in time and space, so that all perturbation quantities oscillate as $\exp(-i\omega t+ik_x x)$ with ω the angular frequency and k_x the lateral wave number.

The resulting ordinary differential equations (5.13) are solved numerically in Sec. VI to determine the z dependence of the magnetosphere's response to oscillatory driving "forces" that are applied in the plasma production plane, $z=0$. In general, the magnetosphere responds with oscillations of its magnetic field and plasma. The oscillations develop into a superposition of downgoing and upgoing plasma waves as they propagate into the regions $z\lesssim -1$ and $z\gtrsim +1$. At $z\ll -1$ and $z\gg +1$, where the equilibrium magnetosphere is homogeneous, the waves can be resolved into MHD modes: a fast magnetosonic mode (which typically carries most of the energy), and two slow magnetosonic modes, which are frozen into the plasma because of the assumption of vanishing plasma pressure. These waves modulate the energy flux carried by the magnetosphere's wind.

Our numerical solutions are restricted to just one equilibrium magnetosphere (an equilibrium shown in Fig. 3), but they cover a wide range of angular frequencies ω and lateral wave numbers k_x, and a complete set of driving "forces" that act in the plasma-production plane, $z=0$. Each driving "force" is characterized by the amplitude f_x of the sinusoidal oscillations of x momentum injected into the magnetosphere, the amplitudes $f_E^{\pm}$ of energy injected upward and downward, and the amplitudes $N^{\pm}$ of plasma rest mass injected upward and downward. The results of the numerical integrations are shown in a huge number of figures: Figs. 5–14; and the numerical methods used are discussed in an appendix. For more detailed presentation of numerical results, see Ref. 15.

Most interesting are injections of x momentum (i.e., f_x driving "forces"), since they correspond most closely to the buffeting pressure of lumpy external **B** fields that push in on a black-hole magnetosphere. For these "forces" the most interesting feature of the numerical solutions is a resonance that shows up in the magnetosphere's response. This resonance occurs when the angular frequency, as measured in the common rest frame of the magnetic field and newly injected plasma, vanishes:

$$\omega_F\equiv\omega-k_x V_F=0\ . \tag{1.3}$$

For a black hole with perturbations $\propto\exp(-i\omega t+im\phi)$, the analogous resonance would be at

$$\omega_F\equiv\omega-m\Omega_F=0\ , \tag{1.4}$$

where Ω_F is the field-line angular velocity, and is roughly equal to half the horizon's angular velocity Ω_H. Correspondingly, if our simple magnetospheric model is a reasonable guide (and it might not be), then the buffeting of the magnetosphere by surrounding, lumpy, accretion-disk **B** fields might produce modulations of the energy flux in the wind and jet at characteristic frequencies $\omega\simeq(m/2)\Omega_H$.

For our simple planar model the resonance shows up both as peaks in the response of the magnetosphere near $z=0$ to the driving force (sharp ridges along the lines $\omega=2k_x$ in Figs. 6–8), and as peaks in the amplification of the perturbations as they propagate from $z=0$ to $z\gg 1$ (sharp ridge in Fig. 13). On resonance, where the magnetosphere's response is strongest, the fractional modulation of the upward energy flux, as measured at $z=0$ in the rest frame of the magnetic field and the newly injected plasma, is

$$\frac{\delta S_z(z=0)}{S_z(z=0)}\simeq 1.15\frac{\delta T_{xz}}{T_{xz}} \tag{1.5a}$$

in our model magnetosphere. Here $\delta T_{xz}/T_{xz}$ is the driving force's fractional modulation of the magnetosphere's momentum flux (stress tensor) at $z=0$. (The quantity f_x is δT_{xz} divided by the upward flux of rest mass in the equilibrium magnetosphere.) During upflow from $z=0$ to $z=+\infty$, the gravitomagnetic-magnetic interaction amplifies the energy flux of the unperturbed magnetosphere by a factor of 80, while amplifying the perturbations by only a factor of 19:

$$\frac{S_z(z\gg 1)}{S_z(z=0)}\simeq 80\ ,\quad \frac{\delta S_z(z\gg 1)}{\delta S_z(z=0)}\simeq 19\ . \tag{1.5b}$$

(If off resonance, this "amplification factor" for perturbations is usually in the range 0.2–3.) Correspondingly, on resonance the distant wind's energy flux is modulated by a factor $1.15\times(19/80)\simeq 0.3$:

$$\frac{\delta S_z(z\gg 1)}{S_z(z\gg 1)}\simeq 0.3\frac{\delta T_{xz}(z=0)}{T_{xz}(z=0)}\ . \tag{1.5c}$$

Thus, on resonance the fractional oscillatory response of the distant wind is roughly equal in magnitude to the fractional oscillatory driving force, while off resonance the response will be far smaller.

For a Kerr hole's magnetosphere, the maximum possible value of the driving force of the buffeting **B** fields is $\delta T_{ij}/T_{ij}\simeq 1$, and it may well be that typical magneto-

spheres are buffeted with $\delta T_{ij} \ll 1$. Thus, if our simple model is a reasonable guide, then the resonant modulation of the wind might not be large enough for detection.

These implications of our calculations for black-hole magnetospheres are discussed more fully in Sec. VII, and possible directions for further research are discussed in Sec. VIII.

II. MODEL SPACETIMES IN WHICH TO STUDY INTERACTIONS OF PLASMA WITH RELATIVISTIC GRAVITY

As was discussed in the Introduction, the dynamics of a black-hole magnetosphere is very complicated to analyze if one insists on using, as the hole's spacetime geometry, the (realistic) Kerr solution to the Einstein field equations. One of the major sources of difficulty is that the analysis must be $2+1$ dimensional (two space dimensions plus one time dimension). Another source of difficulty is the inherent complexity of the MHD equations.

When dealing with vacuum electrodynamics around a black hole, the second difficulty is eased considerably: the vacuum Maxwell equations are far less complex than the MHD equations. Nevertheless, little progress was made on vacuum electrodynamics until Teukolsky[16] eased the first difficulty as well, by showing how to separate variables in the vacuum Maxwell equations and thereby converted the analysis from $2+1$ dimensions to $1+1$.

Since, even in flat spacetime, the MHD equations are inherently far more complex than vacuum Maxwell equations, it seems unlikely that the "complexity" difficulty will ever be eased much for MHD around black holes. It also seems unlikely that the MHD equations will ever be converted into a form, in the Kerr spacetime, that permits reduction from $2+1$ dimensions to $1+1$. In view of this fact, it may be that the most reasonable method to get insight into the dynamics of MHD black-hole magnetospheres is to switch from the realistic Kerr metric to more idealized spacetime metrics that admit a $1+1$ analysis, but still preserve the key features of a rotating black hole.

The key features of a rotating black hole are nicely isolated from each other by a "$3+1$ split" of the spacetime metric:[17,18]

$$ds^2 = -\alpha^2 dt^2 + \gamma_{ij}(dx^i + \beta^i dt)(dx^j dt + \beta^j dt) . \quad (2.1)$$

The quantities α ("lapse function"), β^i ("shift function" or "gravitomagnetic potential"), and γ_{ij} ("spatial metric") can be thought of as three-dimensional scalar, vector, and tensor fields that reside in three-dimensional space (with spatial coordinates x^i) and evolve with the passage of time t. The lapse function α embodies the Newtonian-type gravitational acceleration of the black hole, the gravitational redshift of the ticking rates of clocks, and also the existence and structure of the black-hole horizon (the location at which α goes to zero). The shift function β^i embodies the dragging of inertial frames that is due to rotation of the hole, the storage of rotational energy in the hole's external gravitational field, and it is also the entity by which the rotational energy can be coupled out into electromagnetic fields and particles, thereby driving MHD winds and perhaps amplifying MHD waves. The spatial metric γ_{ij} embodies the geometry of space, both near the hole and far away, and thereby, for example, it produces a significant portion of the deflection of light rays by the hole's gravitational field.

It seems evident that for black-hole magnetospheres the most important of the above phenomena are (i) the storage and release of the hole's rotational energy, as embodied in β^i, and (ii) the hole's Newton-type gravitational attraction and especially its horizon, as embodied in α. Far less important should be the spatial geometry, γ_{ij}.

In order to produce a reasonably simple $(1+1)$-dimensional magnetosphere without losing the key features of a real black hole, then, it seems reasonable to use an idealized, model spacetime in which (i) the spatial metric γ_{ij} is flat, (ii) there is a nonzero shift function β^i—which is inhomogeneous, so its curl, the "gravitomagnetic field"[9] is nonvanishing, (iii) there is a nonzero lapse function α which goes to zero linearly with proper distance from a horizon, and (iv) the shift and lapse functions are invariant under time translations and under displacements along two of the symmetry directions of the flat space (i.e., the full spacetime possesses one temporal and two spatial Killing vector fields). (Here implied is the assumption that the stationary MHD magnetosphere, whose dynamics one wishes to study, has the same symmetry as the gravitational background.) It is this last requirement that will permit the existence of $(1+1)$-dimensional, dynamical MHD magnetospheres. We should also require that far from the horizon the lapse function α and the shift function β^i asymptote to unity and zero, respectively, so the spacetime becomes flat; and, by analogy with a Kerr black hole, α should increase monotonically and the absolute value of β^i should decrease monotonically as one goes outward from the horizon to "infinity."

There are just two types of spacetimes with these properties. In one, α and β^i are invariant under rotational $(\partial/\partial\phi)$ and translational $(\partial/\partial z)$ symmetries; i.e., the spacetime is cylindrical:

$$ds^2 = -\alpha^2(r)dt^2 + dr^2 + dz^2 + r^2[d\phi^2 + \beta(r)dt]^2 . \quad (2.2)$$

In the other, α and β^i are invariant under two translation symmetries ($\partial/\partial x$ and $\partial/\partial y$); i.e., the spacetime is planar:

$$ds^2 = -\alpha^2(z)dt^2 + [dx + \beta(z)dt]^2 + dy^2 + dz^2 . \quad (2.3)$$

In the cylindrical spacetime (2.2) α vanishes at a cylindrical horizon $r = r_H$, and it increases monotonically from 0 to 1 as r goes from r_H to ∞; and β takes on a maximum absolute value, β_H (the cylindrical horizon's angular velocity) at $r = r_H$, and it decreases monotonically to zero as r increases to ∞. In the planar spacetime (2.3) α vanishes at a horizon which we can place at $z = 0$, and it increases monotonically to unity as z increases from 0 to ∞; and the absolute value of β takes on a maximum value, β_H (the horizon's linear velocity relative to infinity) at $z = 0$, and it decreases monotonically to zero at $z \to \infty$. Note that the cylindrical spacetime (2.2) and its station-

ary MHD magnetosphere have the nice feature that as in flat spacetime, so also here, magnetic field lines that thread the horizon will diverge from each other as they reach out to infinity (circumference increases in proportion to radius r). By contrast, the planar spacetime (2.3) and its stationary MHD magnetosphere have the nice computational features that (i) all aspects of the magnetosphere should become asymptotically z independent at large z, and (ii) the nondivergence of magnetic field lines at infinity turns out to push a stationary magnetosphere's fast magnetosonic point off to $z\rightarrow\infty$, thereby saving us from struggling with the computational complexities of smooth transitions through that sonic point.

In this paper we are not even so ambitious as to study MHD magnetospheres in these two model spacetimes. Rather, as a first step in seeking insight into the dynamical MHD interaction of plasmas with rotating-black-hole-type gravity, we shall isolate out just one aspect of the gravitational interaction and study it by itself. Our chosen aspect, of course, will be the shift function β with its storage and release of the spacetime's rotational (or translational) energy. We shall isolate it by working with a modified version of the planar spacetime (2.3) in which the lapse function α is unity everywhere (no horizon; no redshifts),

$$ds^2=-dt^2+[dx+\beta(z)dt]^2+dy^2+dz^2\ , \tag{2.4}$$

while the value of the shift function β decreases monotonically from 0 at $z\rightarrow\infty$ to some constant value (denoted below as $-2V_F$) at $z\rightarrow-\infty$. The specific form we shall use for β is

$$\beta(z)=V_F(\tanh z-1)\ . \tag{2.5}$$

As we shall see, in this very simple spacetime, as in the Kerr spacetime of a real black hole, the shift function β drives an MHD wind which can extract translational energy (rotational energy for Kerr) from the spacetime's gravitational field. Stationary MHD winds in this spacetime are very similar to those in the Kerr metric; and in this spacetime, by contrast with Kerr, it is a manageable problem to study dynamical perturbations of such a wind—the principal objective of this paper.

We should mention that the spacetimes (2.1)–(2.4) are not empty (as can be seen by a straightforward calculation of their Ricci tensor). This is not important for our analyses, however. Because these spacetimes are merely testbeds for studying various aspects of the interaction of relativistic gravity with plasmas, we are free to (and shall) assume that there is no direct, nongravitational interaction between the plasmas we study and the "materials" whose stress energy produce the spacetime curvature.

We regard this paper as just a first step in trying to understand dynamical magnetospheres of black holes. The next, very important step will be to restore a horizon-producing lapse function to the spacetime, i.e., to study MHD in the spacetimes (2.2) and (2.3) rather than (2.4). We shall comment further on this next step in the conclusion of this paper, Sec. VIII below.

III. MHD IN A PLANAR SPACETIME WITH SHIFT BUT NO LAPSE

It is reasonable to expect that in any spacetime with three killing vector fields (one timelike and two spacelike), and for a magnetized dissipation-free plasma, there are MHD equilibrium states whose structure can be analyzed purely algebraically (no differential equations to solve). In this section we shall exhibit an explicit example of this: the algebraic structure of plane-symmetric, stationary flows of a zero-temperature MHD fluid in our model spacetime (2.4). The flows we shall construct will be used in subsequent sections as stationary model "magnetospheres" whose dynamical perturbations are to be studied.

Before proceeding further, let us introduce a few definitions. We will use a 3+1 notation consistent with that of the membrane paradigm,[9] even though we have not included a horizon here. All vector-analysis notations such as the gradient, curl, and vector cross product will be those of the three-dimensional absolute space whose three-metric is δ_{ij}, the Kronecker delta (see Sec. II A of Ref. 19). All quantities will be those measured by FIDO's (fiducial observers), whose four-velocity is

$$\mathbf{n}=\frac{\partial}{\partial t}-\beta\frac{\partial}{\partial x} \tag{3.1}$$

in our model spacetime (2.4). The FIDO-measured fluid velocity of our plasma is described by a spatial vector field lying in the x-z plane:

$$\mathbf{V}=V(z)\mathbf{e}_x+u(z)\mathbf{e}_z\ . \tag{3.2}$$

This fluid velocity is related to the components U^μ of the fluid four-velocity in the coordinate system (2.4) by

$$U^0=\gamma\ ,\quad U^x=\gamma(V-\beta)\ ,\quad U^y=0\ ,\quad U^z=\gamma u\ , \tag{3.3}$$

where γ is the Lorentz factor:

$$\gamma\equiv\frac{1}{\sqrt{1-u^2-V^2}}; \tag{3.4}$$

i.e., the $\mathbf{V}$ of (3.2) is the standard 3+1 embodiment of the four-velocity (3.3). For further details on 3+1 splits of four-dimensional quantities see York,[18] Ref. 9, and the references cited therein. The FIDO-measured magnetic field is also assumed to lie in the x-z plane:

$$\mathbf{B}=B[\lambda(z)\mathbf{e}_x+\mathbf{e}_z]. \tag{3.5}$$

Here B, the z component of $\mathbf{B}$, is a constant as guaranteed by the vanishing divergence of the magnetic field [Eq. (2.6) of Ref. 19; see also Eq. (5.8b) of Ref. 20]. The electric field $\mathbf{E}$ generated by the fluid's motion relative to the FIDO's will be in the y direction:

$$\mathbf{E}=-\mathbf{V}\times\mathbf{B}=E_y\mathbf{e}_y. \tag{3.6}$$

The magnetic field $\mathbf{B}$ and the electric field $\mathbf{E}$ are related to the electromagnetic field tensor $F_{\mu\nu}$ and its dual ${}^*F^{\mu\nu}$ via

$$E^i=-F^i_{\ \mu}n^\mu, \tag{3.7}$$

$$B^i={}^*F^i_{\ \mu}n^\mu. \tag{3.8}$$

We shall assume for simplicity that the plasma has vanishing thermal pressure and vanishing thermal energy density; i.e., we shall restrict ourselves to a "cold plasma," for which the total density of mass-energy ρ and the rest-mass density ρ_0 are the same:

$$p=0\ ,\quad \rho=\rho_0\ , \tag{3.9}$$

and

$$\mu\equiv\frac{p+\rho}{\rho_0}=1. \tag{3.10}$$

This assumption has been used previously, for example, by Michel[21] and by Okamoto[22] in their studies of relativistic stellar winds. In our study it will allow much of the stationary solution to be analyzed analytically, given some additional symmetry requirements.

In our geometry (2.4), the "poloidal" direction, the direction orthogonal to $\boldsymbol{\beta}$, is $\mathbf{e}_z$; so u, B are our V^P, B^P as defined in Ref. 19 [Eq. (3.10) of Ref. 19], and V, λ are our V^T,B^T, the projections of the velocity and magnetic field onto the symmetry direction $\partial/\partial x$. Once we have made this identification, it is very easy to specialize Eqs. (3.27), (3.32), and (3.34) of Ref. 19 to our model and obtain a set of constraints (first integrals) that a stationary MHD configuration must satisfy: From Eq. (3.27) of Ref. 19, we have

$$V=C+\lambda u\ . \tag{3.11}$$

Here,

$$C\equiv\beta+V_F\ , \tag{3.12}$$

and V_F is an integration constant (or "stream function" in the terminology of Phinney[5]), the transverse speed of the frozen-in magnetic field as measured by FIDO's at $z\to\infty$. Notice that the quantity C is nothing but the shift function β, with a constant added onto it; thus, we shall call it the "renormalized shift." Throughout our analysis we shall use C rather than β to embody the spacetime's gravitomagnetic field. In this section we shall not assume the specific form (2.5) for $\beta(z)$, but rather shall allow $\beta(z)$ to be arbitrary (except for the constraint $\beta\to 0$ as $z\to\infty$). Later, in Sec. IV, we shall specialize to the specific form (2.5) with the V_F that appears there set equal to the V_F of (3.12). From Eq. (3.32) of Ref. 19, a result of momentum conservation, we have

$$l=\gamma V-\lambda/s. \tag{3.13}$$

Here l is the (constant, i.e., z-independent) x component of the magnetosphere's linear momentum p_x per unit mass and s is a ratio measuring the relative strength of the magnetic field and the plasma inertia:

$$s\equiv\frac{4\pi\rho\gamma u}{B^2}. \tag{3.14}$$

Because of the conservation of the rest mass,

$$\rho\gamma u=\text{const}, \tag{3.15}$$

and the vanishing divergence of $\mathbf{B}$ ($B=$const), s is another constant. From Eq. (3.34) of Ref. 19, a result of the conservation of energy and momentum, we have

$$f=\gamma(1-CV). \tag{3.16}$$

Here f is also a constant, representing the specific energy measured by an "imaginary" observer who is comoving with the frozen-in magnetic field. The observer is "imaginary" because on one side of the light planes ($|C|\geq 1$), the field moves faster than the speed of the light. Notice that the constants V_F, l, s, f are all dimensionless.

Equations (3.4), (3.11), (3.13), and (3.16) can be combined into a single quartic equation for one of the stationary, dimensionless quantities u, V, or λ; we shall choose the combination γu. This quartic equation will be solved to obtain a stationary configuration: the quantity γu as a function of the renormalized shift C and the constant parameters s, l, f (which are regarded as specified beforehand); and then via Eqs. (3.11), (3.17), and (3.18), the quantities u, V, λ. In this procedure the z dependence of the equilibrium configuration will arise solely through the renormalized shift function $C(z)$.

More specifically, we first use (3.11) and (3.16) to eliminate V and λ from (3.13) and obtain an expression for γ in terms of γu, C, and the (specified) constant parameters s, l, and f,

$$\gamma=\frac{(Cl+f)\gamma u-f/s}{\gamma u-(1-C^2)/s}. \tag{3.17}$$

In turn, Eq. (3.17) is substituted into (3.16), resulting in a similar expression for γV:

$$\gamma V=\frac{\gamma ul-fC/s}{\gamma u-(1-C^2)/s}. \tag{3.18}$$

The quartic equation for $\gamma u(C,s,l,f)$, obtained by combining (3.4), (3.17), and (3.18), is the following "wind equation" [see Eqs. (3.46) and (3.47) of Ref. 19; also Eqs. (IV,8.5), (V,5.1) of Phinney[5] and Eq. (3.12) of Kennel, Fujimura, and Okamoto[23]]:

$$D\equiv K\frac{(\gamma u-F_1)(\gamma u-F_2)}{(\gamma u-F_3)^2}-(\gamma u)^2-1=0. \tag{3.19a}$$

Here,

$$K\equiv(f+Cl)^2-l^2, \tag{3.19b}$$

$$F_1\equiv\frac{1-C}{f+Cl-l}\frac{f}{s}, \tag{3.19c}$$

$$F_2\equiv\frac{1+C}{f+Cl+l}\frac{f}{s} \tag{3.19d}$$

$$F_3\equiv\frac{1-C^2}{s}. \tag{3.19e}$$

As we can see, the wind equation (3.19) is quartic in γu, so it generally has 0, 2, or 4 real solutions. It has an apparent singular point at $\gamma u=F_3$, or

$$s\gamma u+C^2-1=0. \tag{3.20}$$

This is the Alfvén point, i.e., the point at which the phase velocity of short-wavelength, small-amplitude Alfvén waves is the same as the fluid speed.[5,23] However, it turns out that the MHD wind can always pass through this "critical point" smoothly (see Phinney[5] for a detailed discussion). There is another singular point hidden in the

denominator of the derivative of γu with respect to C. By rewriting (3.4) [or (3.19a)] as

$$D=\gamma^2-\gamma^2V^2-\gamma^2u^2-1$$
$$=\gamma^2-\left[\frac{f-\gamma}{C}\right]^2-\gamma^2u^2-1=0$$

and differentiating it with respect to C, we obtain

$$\frac{\partial \ln(\gamma u)}{\partial \ln C}=\frac{\gamma u\left[\frac{\partial D}{\partial C}\right]_{\gamma u}}{C\left[\frac{\partial D}{\partial \gamma u}\right]_C}$$
$$=\frac{(\gamma V)^2(s\gamma u+C^2-1)+\lambda\gamma u(sl\gamma u-2\gamma C)}{(\gamma u)^2(s\gamma u+C^2-1-\lambda^2)}. \tag{3.21}$$

Because of the assumption of zero thermal pressure, no slow magnetosonic waves are present in our model and the factor $(\gamma u)^2$ in the denominator is just a reminder that there is no slow magnetosonic critical point for our plasma flow to cross. The point where the other factor vanishes,

$$s\gamma u+C^2-1-\lambda^2=0, \tag{3.22}$$

is the fast magnetosonic point.[5,23] It will look familiar if we rewrite $s\gamma u$ as $4\pi\rho\gamma^2u^2/B^2$. This point is also where the two positive solutions for γu meet and terminate. (See, for example, Sec. 7.5 of Ref. 23.)

Shown in Fig. 1 are solutions of (3.19) for a particular set of parameters s, l, and f. By making a one-to-one monotonic map of the "normalized shift" C to the z coordinate [such as Eqs. (2.5) and (3.12)], we can reexpress these solutions as functions of height z: $\gamma u=\gamma u(z)$. The solution of interest to us is the "wind" branch (b) along which γu increases monotonically from much less than the Alfvén speed, through the Alfvén speed, and up toward the fast magnetosonic speed. If $V_F\equiv C_\infty$ is equal to C_0, then the wind speed approaches the fast magnetosonic speed as $z\to\infty$ [curve (b) of Fig. 2]. If $V_F<C_0$, then the wind asymptotes to a speed less than fast magnetosonic speed [curve (c) of Fig. 2(a)]. If $V_F>C_0$, then the MHD outflow terminates before it reaches spatial infinity, resulting in a nonphysical solution [curve (a) of Fig. 2].

By using the schematic method employed in Kennel, Fujimura, and Okamoto,[23] we can convince ourselves that Figs. 1 and 2 are quite generic; they depict schematically solutions of (3.19) for a general set of s, l, f (and V_F). In other words, for all s, l, f, we always have as in Fig. 1 a positive, increasing (with C) "wind" branch that meets with another positive branch from below at the fast magnetosonic point C_0 and terminates there. The Alfvén point, where these two positive branches intersect, is inside the "light plane," i.e., the plane where the electromagnetic field moves at the speed of light ($C=1$). The other positive branch always changes sign at the "light plane." We also have a negative branch that approaches to a large negative value very quickly.

We shall not present here an analysis of our model similar to the analysis in Ref. 22. Instead, we shall look at the wind equation and the constraints it places on stationary configurations in regions of the flow where C is very small and where it is very large. The resulting equations are not very useful as approximations in their own right. But they do give us some hint on how the characteristics of the wind solutions change with the flow constants s, l, f (and V_F).

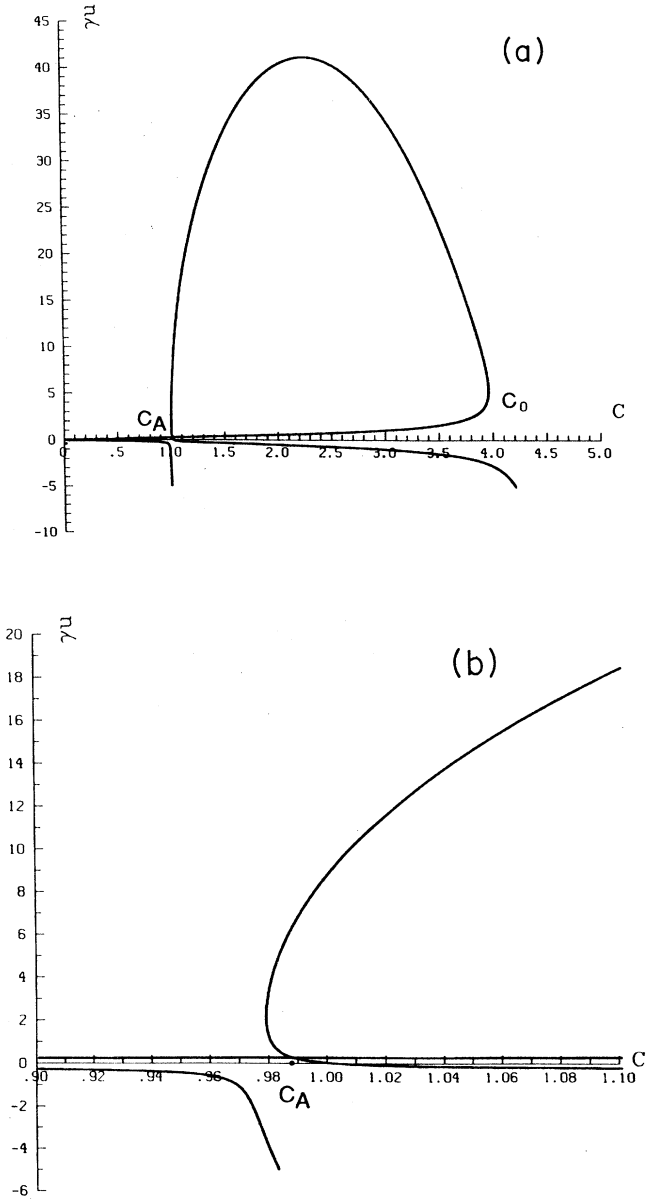

FIG. 1. Solutions $\gamma u(C)$ to Eq. (3.19) for $s=0.1$, $l=40$, $f=1.01$. The "light plane" where $C=1$ is outside the Alfvén point C_A, the location where the two positive branches cross each other. The fast magnetosonic point where the positive branches meet and terminate in this cold plasma model is located at $C_0=3.94$. (a) Diagram showing both sonic points; (b) diagram showing details near the Alfvén point $C_A\simeq 0.988$.

Focus attention, first, on the region of the flow (near $z=0$ in the models of Sec. IV) where $C \ll 1$. We shall assume that the flux of conserved x momentum ($\mathbf{S}^P_{P_\xi}$ of Ref. 19) is mostly in the electromagnetic field, $l \gg 1$. We shall also assume that $(sl)^2 \gg 1$. The role of this product sl will become evident later at the end of this section. Since we are interested in the "wind" branch where γu increases with C, we shall regard this as the region in which the flow "starts." Restrict attention to flows for which, at $C=0$, the plasma velocity is small and thus γ is near unity. Since $\gamma = f$ when $C=0$ [Eq. (3.16)], such flows must have

$$\Delta f \equiv f - 1 \ll 1 , \tag{3.23}$$

and at $C=0$,

$$(\gamma u)^2 \simeq u^2 \lesssim 2\Delta f \ll 1. \tag{3.24}$$

Thus, Δf determines how fast the flow starts out at $C=0$. In the region of small C we shall denote $C \equiv \epsilon$. The region of interest will be

$$C \equiv \epsilon \lesssim \sqrt{\Delta f} \ll 1 \ll l. \tag{3.25}$$

In this region we would expect that

$$u, V \sim \epsilon \lesssim \sqrt{\Delta f} \ll 1 \ll l. \tag{3.26}$$

Indeed, this is the case: We rewrite (3.16) as

$$\Delta f = \tfrac{1}{2}u^2 + \tfrac{1}{2}V^2 - \epsilon V. \tag{3.27}$$

Combining this with (3.11) and (3.13) we immediately have

$$u = \left[\frac{2\Delta f + \epsilon^2}{1 + s^2 l^2} \right]^{1/2}, \tag{3.28a}$$

and

$$V = \epsilon - sl \left[\frac{2\Delta f + \epsilon^2}{1 + s^2 l^2} \right]^{1/2}, \tag{3.28b}$$

$$\lambda = -sl + s \left[\epsilon - sl \left[\frac{2\Delta f + \epsilon^2}{1 + s^2 l^2} \right]^{1/2} \right]. \tag{3.28c}$$

Notice that for $sl > 0$, V starts out negative (because of the strong dragging of inertial frames there) and then changes sign at $\epsilon \sim \sqrt{\Delta f}$. As ϵ gets larger, moving into the region $1 \gg \epsilon^2 \gg \Delta f$,

$$u \simeq \frac{\epsilon}{\sqrt{1 + s^2 l^2}}, \tag{3.28a'}$$

$$V \simeq \frac{\epsilon}{2 s^2 l^2}, \tag{3.28b'}$$

$$\lambda \simeq -sl + \frac{\epsilon}{2sl^2}. \tag{3.28c'}$$

We see that when the product sl is large, the fluid will be difficult to accelerate and when l is also large, the frozen-in magnetic field lines can hardly be bent as C (i.e., β) changes.

Turn, next, to the region of the flow in which $C \gg 1$. In this region the wind equation (3.19) shows that this same product, sl, together with $V_F (\equiv C_\infty)$, determines whether a particular stationary solution can reach spatial infinity. At

$$C \gg 1 ,$$

the wind equation can be approximated as

$$(Cl)^2 \left[(\gamma u)^2 - \frac{f^2}{(sl)^2} \right] \simeq [(\gamma u)^2 + 1] \left[\gamma u + \frac{C^2}{s} \right]^2 . \tag{3.29}$$

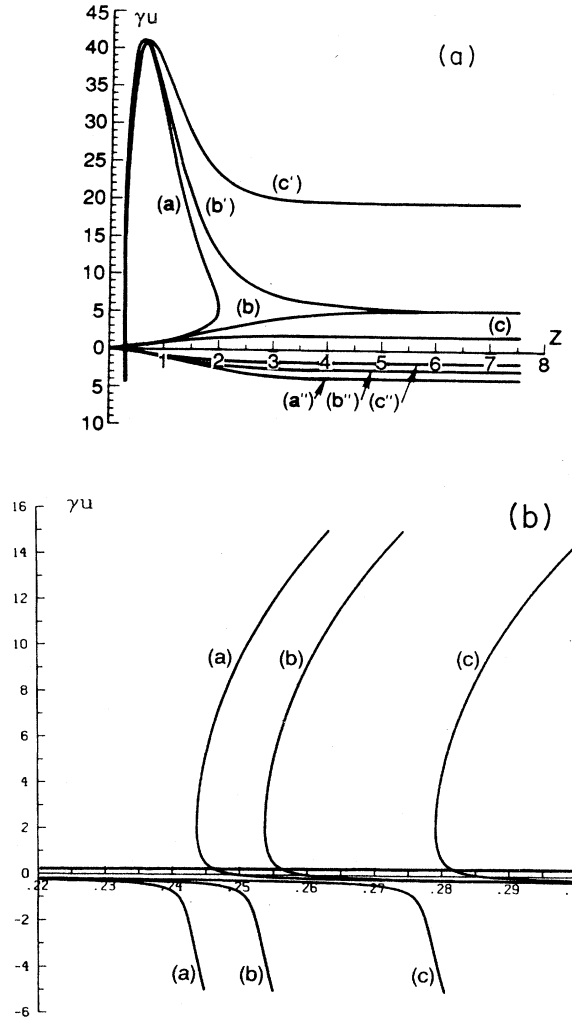

FIG. 2. The same stationary solution as in Fig. 1, drawn as a function of the coordinate z, with β (or C) the monotonic increasing function of z given by Eqs. (2.5) and (3.12). The solution is shown for three different values of $C_\infty \equiv V_F$, the value of C at $z \to \infty$. Curves (c) and (c') correspond to $C_\infty > C_0$, which permits the stationary "wind" solution [curve (c)] to reach spatial infinity at a flow speed smaller than the fast magnetosonic speed there. Curves (b) and (b') correspond to $C_\infty = C_0$, the critical value of C_∞ that enables the (continuously increasing) "wind" branch of the solution [curve (b)] to approach the fast magnetosonic speed at spatial infinity. Curve (a) corresponds to $C_\infty < C_0$, an unphysical case in which the wind branch terminates at finite z. (a) Stationary solutions in the range $0 \le z < 7.5$; (b) stationary solutions near the Alfvén point.

By definition,

$$s\gamma u=\frac{4\pi\rho\gamma^2u^2}{B^2}>0;$$

therefore,

$$\left[\gamma u+\frac{C^2}{s}\right]^2>\left[\frac{C^2}{s}\right]^2.$$

Using this inequality, we can reduce (3.29) to the form

$$[(sl)^2-C^2](\gamma u)^2\gtrsim C^2.$$

Hence, the following inequality holds:

$$(sl)^2\gtrsim C^2, \tag{3.30}$$

which means that the product sl must be large enough in order for the wind equation to have any positive solutions at C. For a wind with fixed V_F to reach spatial infinity in a given gravitational background, either we should have s large enough so the fluid initially (at $C\ll 1$) will have enough inertia that its speed cannot be accelerated beyond the fast magnetosonic speed; or we should have l big enough so the magnetized fluid will have enough x-momentum stored in the magnetic field to be converted into the (particle) energy (via the shift function) to make its mass inertia become large at $C\gg 1$.

IV. STATIONARY MHD "MAGNETOSPHERE"

It is generally believed that in or near the ergosphere of a rotating, magnetized black hole, electron-positron pairs are created by high-energy photons, electrons, or protons with the help of the magnetic field or its coupling to the gravitomagnetic field of the rotating hole.[3,5–7,9] Part of the resulting electron-positron-pair plasma flows into the horizon, and part is driven out to infinity as a steady MHD wind.[3,5,8] When this MHD wind is dynamically perturbed, e.g., by the pressure of chaotic magnetic fields anchored in the hole's accretion disk, there will result MHD waves that ride on top of and modulate the wind's steady flow. In Secs. V and VI we shall study such MHD waves. But first, in this section, we shall prepare for that study by building explicit models for the stationary, MHD background flow. Throughout, we shall restrict attention to the planar model spacetime (2.4).

To model the background flow, we use the stationary solutions derived in the previous section and assume the following to join solutions in the positive-z half-plane with those in the negative-z half-plane:

$$\mathbf{V}(-z)=-\mathbf{V}(z),\quad \rho(-z)=\rho(z)\ , \tag{4.1}$$

$$\mathbf{B}(-z)=\mathbf{B}(z), \tag{4.2}$$

$$\beta'(-z)=\beta'(z)\ \text{ and } \beta(z)\text{ is continuous across } z=0. \tag{4.3}$$

It is not hard to verify the following transformation rules for the flow constants on both sides of the $z=0$ plane under the above assumptions:

$$s^+=-s^-, \tag{4.4a}$$

$$l^+=-l^-, \tag{4.4b}$$

$$f^+=f^-. \tag{4.4c}$$

Here the superscripts $+$ indicate that those flow constants are in the $z>0$ half-plane, while the superscripts $-$ indicate those in the $z<0$ half-plane. In the following, we will drop the superscripts $+$ and $-$ for the flow constants and refer to them using their values in the $z>0$ half-plane, unless explicitly specified otherwise.

The MHD flow is intended to model a wind flowing out of the ergosphere of a Kerr black hole and also an accretion flow down to the horizon, both originated in the ergosphere, so we will choose

$$C=0\ \text{ at } z=0\ . \tag{4.5}$$

In other words, we assume in our model the pair production region to be delta-function sources and put this production plane at the origin, $z=0$. Thus, the MHD plasma will emerge from $z=0$ and will flow from there in both directions, to $z\to-\infty$ and to $z\to+\infty$. In our planar model, the magnetic field lines do not diverge from each other at infinity, so no steady, continuous solution exists beyond the fast magnetosonic critical point (see Sec. III; see also Ref. 22). This means that in order for our wind to reach infinity, we must choose parameters s,l,V_F such that the flow speed never exceeds, and at most approaches, that of the fast magnetosonic waves at the spatial infinity. In other words, the chosen parameters s, l are such that the maximumly allowed "normalized shift" C_0 determined from s and l for the wind branch will be no larger than V_F, the asymptotic value of C (see Fig. 2). We would like our plasma-production region ($C=z=0$) to resemble the ergosphere of a black hole, in that no object there can remain at rest relative to "infinity"; i.e., the "dragging of inertial frames" is so strong that $|\beta|\geq 1$ there. These considerations will considerably restrict our choice of V_F.

Under the condition $C(z=0)=0$, we have, for the Lorentz factor of our stationary flow, $\gamma=f$ at the origin, where the flow starts. We shall not choose $f=1$ because that would force u to vanish at $z=0$ and (since $\rho\gamma u=\text{const}$) would also force the plasma density ρ to be infinite there—and that, in turn, would prevent MHD waves from propagating across the plasma production region $z=0$. Instead, we will choose

$$\Delta f\equiv f-1\ll 1 \tag{3.23}$$

so that the wind can start at a small but finite speed. Because of our assumption (4.1), the flow velocity is not continuous across $z=0$. The jumps in the flow velocity and in other MHD quantities at $z=0$ must satisfy a set of junction conditions that depend on the details of the delta-function source of plasma. The junction conditions at the interface are actually just a special form of the MHD equations there. They can be derived from the MHD equations or from combinations of them, using the standard pillbox or tiny integration-loop method. From the conservation of the magnetic flux [Eq. (2.6) of Ref. 19], this method gives

$$[B_z]=0. \tag{4.6}$$

Here and below square brackets denote the jump: $[B_z]\equiv B_z(\text{just above } z=0)-B_z(\text{just below } z=0)$. From Ampere's law [Eq. (2.5) of Ref. 19], we obtain

$$[E_y]\equiv[B_zV_x-B_xV_z]=0. \tag{4.7}$$

From the conservation of the rest mass (or baryon number) [Eq. (2.24) of Ref. 19], we obtain

$$[\rho\gamma V_z]=\dot{M}\ . \tag{4.8}$$

From the conservation of energy measured locally by FIDO's at the origin (i.e., the conservation of the projection of four-momentum on the Killing vector $\partial/\partial t-V_F\partial/\partial x$), we obtain

$$[\rho\gamma^2V_z]+\frac{1}{4\pi}(V_zB_x-V_xB_z)[B_x]=\dot{E}. \tag{4.9}$$

From the conservation of the x component of momentum, we obtain

$$[\rho\gamma^2V_xV_z]-\frac{B_z}{4\pi}[B_x]=\dot{P}. \tag{4.10}$$

In the above equations, we have used the following definitions for our delta-function sources at $z=0$:

$\dot{M}\equiv$ (rest-mass injection rate at $z=0$ per unit area, per unit FIDO time), (4.11a)

$\dot{E}\equiv$ (injection rate at $z=0$ per unit area, per unit FIDO time of energy measured by FIDO's), (4.11b)

$\dot{P}\equiv$ (injection rate at $z=0$ of x-momentum per unit area, per unit FIDO time). (4.11c)

Note: Because the lapse function is unity everywhere, proper time as measured by the FIDO's ("FIDO time") is everywhere equal to coordinate time t. We can also combine $\dot{M}$ and $\dot{E}$ to get $\dot{E}_K\equiv\dot{E}-\dot{M}$, the injection rate of the kinetic energy measured locally by the FIDO's and obtain a junction condition involving $\dot{E}_K$:

$$[\rho\gamma(\gamma-1)V_z]+\frac{1}{4\pi}(V_zB_x-V_xB_z)[B_x]=\dot{E}_K. \tag{4.9'}$$

By specializing to our stationary configuration [Eq. (3.6) and our assumption on the pair-production plane (4.5)], we obtain

$$E_y(z=0)=C(z=0)B=0\ . \tag{4.12}$$

This, combined with the junction condition (4.6) and the definition of V_F (3.12), implies

$$B[V_F]=B[C]=[E_y]=0. \tag{4.13}$$

Therefore, the continuity of the electric field (produced by the fluid's motion under our perfect MHD assumption) forces V_F to be the same on both sides of the interface. Since we assume for the stationary configuration that $V_z^+=-V_z^-$, the stationary flow carries away the mass injected at the interface equally to both sides,

$$\dot{M}=[\rho\gamma u]=2\rho\gamma u^+=-2\rho\gamma u^-. \tag{4.14}$$

Since we have also chosen $\lambda^+=\lambda^-$, no net force in the x direction acts on the exiting stationary flow: i.e.,

$$\dot{P}=[\rho\gamma^2uV]-\frac{B^2}{4\pi}[\lambda]=0; \tag{4.15}$$

and the injected energy

$$\dot{E}=[\rho\gamma^2u]+\frac{B^2}{4\pi}(\lambda u-V)[\lambda]=\rho f^2[u], \tag{4.16a}$$

or

$$\dot{E}_K=\rho f(f-1)[u] \tag{4.16b}$$

is completely in the fluid's motion and is carried away equally to both sides. The Poynting flux, however, is guaranteed to be continuous by the vanishing of the electric field [Eqs. (4.5)] at the interface.

Figure 3 shows a schematic representation of this background, equilibrium flow, upon which we shall study MHD perturbations. The downward "wind" solution (i.e., downward flowing stationary solution) on the $z<0$ side is constructed from the "wind" branch of Fig. 1 on

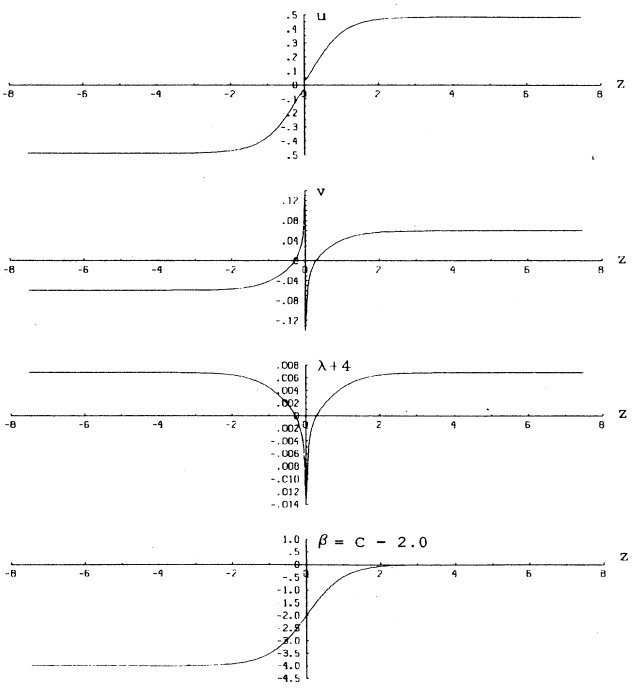

FIG. 3. A stationary gravitational and MHD background, with reflection symmetries (4.1)–(4.3), for the parameter set $s=0.1$, $l=40$, $f=1.01$, and $V_F=2$.

the $z>0$ side, using the symmetries (4.1)–(4.3). In this figure, and henceforth, we specialize to the specific shift function (2.5):

$$\beta(z)=V_F\ (\tanh z-1),\quad C(z)=V_F\tanh z. \tag{2.5}$$

The parameters s, l, f, and V_F are such that the asymptotic speeds of the background flow at the two infinities are less than the fast magnetosonic speed, and the flow starts at a finite speed at $z=0$. Because of the monotonic, one-to-one nature of map (2.5) from the shift function to the z coordinate, and because of the general form of γu as functions of the "normalized shift" C (Fig. 1), this particular stationary background flow does not cross any magnetosonic points. (Note that because of the assumption of zero thermal pressure, the slow magnetosonic speed degenerates to the flow speed.) This will save us from the trouble of passing waves through their sonic points when we later study the dynamic perturbations numerically in Sec. VI.

As a last point we wish to mention here that although our chosen spacetime has no horizon (thereby permitting a study of shift-function effects in isolation), we can think of the region $z\to-\infty$ as analogous to a horizon. This viewpoint is justified by the fact that a black-hole horizon behaves very much like an "infinity" (as one sees from analyses using the Regge-Wheeler[24] "tortoise coordinate,"[25] and as Punsly and Coroniti[13] emphasize in their approach to black-hole magnetospheres). If the flow is chosen to asymptotically approach the fast-magnetosonic speed, then this viewpoint is reinforced by the fact that no information can propagate in from $z=-\infty$ via any kind of MHD wave. It will be instructive, in future research, to test this viewpoint that $z\to-\infty$ is analogous to a horizon by comparing MHD flows in the horizon-endowed model spacetime (2.3) with those in our horizon-free spacetime (2.4).

V. MHD WAVES IN THE "MAGNETOSPHERE": ANALYTIC ANALYSIS

We turn, now, to perturbations of the steady "magnetospheres" constructed in Sec. IV. For ease of analysis we shall assume that the amplitude of the perturbations is small, and we shall linearize in that amplitude. In this section we shall develop the linearized, analytic theory of the perturbations, and then in Sec. VI we shall describe numerical solutions to the perturbation equations.

This section is divided into subsections. In Sec. V A we present the perturbation equations in the time domain, and we present the junction conditions which the perturbations must satisfy at the location, $z=0$, of the background flow's discontinuity. In Sec. V B we specialize to monochromatic perturbations, i.e., to perturbations with dependences $e^{-i\omega t}e^{ik_x x}$ on t and x. In Sec. V C we derive and discuss a complete set of solutions to the perturbation equations at spatial infinity, where the background flow and the shift function are constant. These "solutions at infinity" will be used in Sec. VI as checks on the asymptotic forms of our numerical solutions for MHD waves in the magnetosphere.

A. Perturbation equations and junction conditions

For simplicity we shall confine attention to magnetospheres in which the perturbed flow, like the steady background flow, has its magnetic field and velocity entirely in the x-z plane and is symmetric in the y direction (no dependence of perturbed quantities on y). However, the waves can propagate in any direction in the x-z plane and thus must depend on x and z as well as on time t. We shall characterize the perturbed MHD flow by its velocity $\mathbf{V}$ and magnetic field $\mathbf{B}$ as measured by the FIDO's, and the fluid's density ρ as measured in the fluid's rest frame. More specifically, $\mathbf{V}$ is related to the components of the FIDO's four-velocity by the standard relation (3.3); $\mathbf{B}$ is related to the components of the Maxwell tensor by the standard relations (3.8); and ρ is the density of rest mass and also the density of total fluid mass energy as measured in the fluid's local rest frame. The unperturbed quantities will be denoted by a superscript zero when otherwise there would be ambiguities. The first-order perturbations in these quantities we shall denote by $\delta\mathbf{V}$, $\delta\mathbf{B}$, and $\delta\rho$.

We shall use the following dimensionless notation for the perturbation quantities: For the magnetic-field perturbation $\delta\mathbf{B}$ and density perturbation $\delta\rho$, we define b_x, b_z, and $\tilde{\rho}$ by

$$\mathbf{b}\equiv\delta\mathbf{B}/B=b_x(t,x,z)\mathbf{e}_x+b_z(t,x,z)\mathbf{e}_z, \tag{5.1}$$

$$\tilde{\rho}\equiv\delta\rho/\rho=\tilde{\rho}(t,x,z). \tag{5.2}$$

The velocity perturbation $\delta\mathbf{V}$ is already dimensionless in our geometric units where $G\equiv c\equiv 1$, so we define v_x and v_z by

$$\mathbf{v}\equiv\delta\mathbf{V}=v_x(t,x,z)\mathbf{e}_x+v_z(t,x,z)\mathbf{e}_z. \tag{5.3}$$

The general-relativistic MHD equations in a general, well-behaved background spacetime were written down in Ref. 19 [Eqs. (2.5), (2.13), (2.22), and (2.24)]. Because our specific spacetime has such a simple metric, (2.4), all the gravitational quantities in those equations are zero except the derivative of β. Our simple equation of state $\mu=1$ [Eq. (3.10)], and the assumption of confining $\mathbf{B}$ and $\mathbf{V}$ to the x-z plane also simplify the MHD equations considerably. For example, the full equation describing force balance becomes

$$\left[\left(\rho\gamma^2+\frac{\mathbf{B}^2}{4\pi}\right)\delta_{ij}+\rho\gamma^4V_iV_j-\frac{1}{4\pi}B_iB_j\right]\left[\frac{\partial}{\partial t}-\boldsymbol{\beta}\cdot\boldsymbol{\nabla}\right]V^j+\frac{1}{4\pi}\left[\mathbf{B}\times\left\{\mathbf{V}\times\left[\left[\frac{\partial}{\partial t}-\boldsymbol{\beta}\cdot\boldsymbol{\nabla}\right]\mathbf{B}\right]\right\}\right]_i$$
$$+\rho\gamma^2V_{i,j}V^j+\rho\gamma^4V_iV_{j,k}V^jV^k=\rho\gamma^2\beta_{j,i}V^j+\frac{1}{4\pi}(B_{i,j}B^j-B_{j,i}B^j). \tag{5.4}$$

By invoking the above facts, substituting

$$\mathbf{B}=\mathbf{B}^0+\delta\mathbf{B},\quad \mathbf{V}=\mathbf{V}^0+\delta\mathbf{V},\quad \rho=\rho^0+\delta\rho,$$

and

$$\gamma=\frac{1}{\sqrt{1-u^2-V^2}}+\frac{\mathbf{V}^0\cdot\delta\mathbf{V}}{(1-u^2-V^2)^{3/2}}$$

into the general-relativistic MHD equations [Eqs. (2.5), (2.13), and (2.24) of Ref. 19 and Eq. (5.4) above], and keeping only terms linear in the perturbations, we obtain the following form of the perturbed MHD equations in terms of the dimensioned perturbations $\delta\mathbf{V}$, $\delta\mathbf{B}$, $\delta\rho$:

$$\left[\frac{\partial}{\partial t}-\boldsymbol{\beta}\cdot\nabla\right]\delta\mathbf{B}=\nabla\times(\mathbf{v}\times\mathbf{B})+\nabla\times(\mathbf{V}\times\delta\mathbf{B})-\delta\mathbf{B}\cdot\nabla\boldsymbol{\beta}, \tag{5.5a}$$

$$\nabla\cdot(\delta\mathbf{B})=0, \tag{5.5b}$$

$$\begin{aligned}&\left[\left[\rho\gamma^2+\frac{\mathbf{B}^2}{4\pi}\right]\delta_{ij}+\rho\gamma^4V_iV_j-\frac{1}{4\pi}B_iB_j\right]\left[\frac{\partial}{\partial t}-\boldsymbol{\beta}\cdot\nabla\right]v^j+\frac{1}{4\pi}\left[\mathbf{B}\times\left\{\mathbf{V}\times\left[\left[\frac{\partial}{\partial t}-\boldsymbol{\beta}\cdot\nabla\right]\delta\mathbf{B}\right]\right\}\right]_i\\&\quad+\rho\gamma^2v_{i,j}V^j+\rho\gamma^4V_iv_{j,k}V^jV^k-\frac{1}{4\pi}(\delta B_{i,j}-\delta B_{j,i})B^j\\&\qquad=\gamma^2[\delta\rho V^j+2\rho\gamma^2(\mathbf{V}\cdot\mathbf{v})V^j+\rho v^j]\beta_{j,i}-\rho\gamma^4(v_iV^j+V_iv^j)V_{k,j}V^k+\frac{1}{4\pi}(B_{i,j}-B_{j,i})\delta B^j\\&\qquad\quad-\gamma^2[\delta\rho V^j+2\rho\gamma^2V^j(\mathbf{V}\cdot\mathbf{v})+\rho v^j]V_{i,j}-\gamma^4V_i[\delta\rho V^j+4\rho\gamma^2V^j(\mathbf{V}\cdot\mathbf{v})+\rho v^j]V_{j,k}V^k,\end{aligned} \tag{5.5c}$$

$$\begin{aligned}&\left[\frac{\partial}{\partial t}-\boldsymbol{\beta}\cdot\nabla+\mathbf{V}\cdot\nabla\right]\delta\rho-\frac{\delta\rho}{\rho}\mathbf{V}\cdot\nabla\rho+\rho\gamma^2\mathbf{V}\cdot\left[\left[\frac{\partial}{\partial t}-\boldsymbol{\beta}\cdot\nabla+\mathbf{V}\cdot\nabla\right]\mathbf{v}\right]+\rho\nabla\cdot\mathbf{v}\\&\qquad=-2\rho\gamma^2(\mathbf{V}\cdot\mathbf{v})\mathbf{V}\cdot\nabla(\ln\gamma)-\rho\gamma^2(\mathbf{V}\cdot\nabla\mathbf{V})\cdot\mathbf{v}+\rho\mathbf{v}\cdot\nabla(\ln u).\end{aligned} \tag{5.5d}$$

In deriving (5.5d), we also need Eq. (3.15) ($\rho\gamma u=$const) to eliminate derivatives of ρ. Rewritten explicitly in component form and using the dimensionless version of the perturbation variables (b_x, b_z, v_x, v_z, $\tilde{\rho}$), these perturbation equations take the form

$$\frac{db_x}{d\tau}+Vb_{x,x}+ub_{x,z}=-u'b_x+(V-\beta)'b_z+v_{x,z}-\lambda v_{z,z}-\lambda' v_z, \tag{5.6a}$$

$$\frac{db_z}{d\tau}+Vb_{z,x}+ub_{z,z}=\lambda v_{z,x}-v_{x,x}, \tag{5.6b}$$

$$b_{x,x}+b_{z,z}=0, \tag{5.6c}$$

$$\begin{aligned}&\left[\frac{B^2}{4\pi}+\rho\gamma^2(1+\gamma^2V^2)\right]\frac{dv_x}{d\tau}+\left[\rho\gamma^4uV-\frac{\lambda B^2}{4\pi}\right]\frac{dv_z}{d\tau}+\left[\rho\gamma^2(1+\gamma^2V^2)-\frac{B^2}{4\pi}\right](Vv_{x,x}+uv_{x,z})\\&\quad+\left[\rho\gamma^4uV+\frac{\lambda B^2}{4\pi}\right](Vv_{z,x}+uv_{z,z})-\frac{B^2}{2\pi}uVb_{z,z}+\frac{B^2}{4\pi}[(1-V^2)b_{z,x}-(1-u^2)b_{x,z}]\\&\qquad=-\frac{B^2}{4\pi}uu'b_x+\frac{B^2}{4\pi}[\lambda'+u(V-\beta)']b_z-\rho\gamma^2u[(1+\gamma^2V^2)V'+\gamma^2uVu']\tilde{\rho}\\&\qquad\quad-\rho\gamma^4u[(1+4\gamma^2V^2)uu'+4(1+\gamma^2V^2)VV']v_x\\&\qquad\quad-\left[\frac{B^2}{4\pi}u\lambda'+\rho\gamma^2[(1+2\gamma^2u^2)(1+2\gamma^2V^2)-\gamma^2V^2]V'+2\rho\gamma^4(1+2\gamma^2u^2)uVu'\right]v_z,\end{aligned} \tag{5.6d}$$

$$\left[\frac{\lambda^2B^2}{4\pi}+\rho\gamma^2(1+\gamma^2u^2)\right]\frac{dv_z}{d\tau}+\left[\rho\gamma^4uV-\frac{\lambda B^2}{4\pi}\right]\frac{dv_x}{d\tau}+\left[\rho\gamma^2(1+\gamma^2u^2)-\frac{\lambda^2B^2}{4\pi}\right](Vv_{z,x}+uv_{z,z})$$
$$+\left[\rho\gamma^4uV+\frac{\lambda B^2}{4\pi}\right](Vv_{x,x}+uvxz)+\frac{\lambda B^2}{2\pi}uVb_{z,z}-\frac{\lambda B^2}{4\pi}[(1-V^2)b_{z,x}-(1-u^2)b_{x,z}]$$
$$=-\frac{B^2}{4\pi}(\lambda'-\lambda uu')b_x-\frac{\lambda B^2}{4\pi}u(V-\beta)'b_z-\rho\gamma^2[(1+\gamma^2u^2)uu'+\gamma^2u^2VV'-V\beta']\tilde{\rho}$$
$$-\rho\gamma^2[\gamma^2u^2(1+4\gamma^2V^2)V'-(1+2\gamma^2V^2)\beta'+2\gamma^2uV(1+2\gamma^2u^2)u']v_x$$
$$-\left[\rho\gamma^2(1+\gamma^2u^2)(1+4\gamma^2u^2)u'+2\rho\gamma^4(1+2\gamma^2u^2)uVV'-2\rho\gamma^4uV\beta'-\frac{\lambda B^2}{4\pi}u\lambda'\right]v_z, \quad (5.6e)$$

$$\frac{d\tilde{\rho}}{d\tau}+V\tilde{\rho}_{,x}+u\tilde{\rho}_{,z}+\gamma^2V\frac{dv_x}{d\tau}+\gamma^2u\frac{dv_z}{d\tau}+(1+\gamma^2V^2)v_{x,x}+(1+\gamma^2u^2)v_{z,z}+\gamma^2uV(v_{x,x}+v_{z,x})$$
$$=-\gamma^2u[(1+2\gamma^2V^2)V'+2\gamma^2uVu']v_x+[(1-2\gamma^2u^2)(1+\gamma^2u^2)u'/u-2\gamma^4u^2VV']v_z. \quad (5.6f)$$

In these equations, a comma denotes a partial derivative, a prime denotes a derivative with respect to z, and $(d/d\tau)\equiv(\partial/\partial t-\beta\partial/\partial x)$ is the time derivative in the FIDO's frame. These equations are to be solved together with the following set of junction conditions at $z=0$, where the background flow is discontinuous:

$$[b_z]=0, \quad (5.7a)$$

$$[v_x]-\lambda[v_z]-u\{b_x\}+2\lambda ub_z=0, \quad (5.7b)$$

$$\{\tilde{\rho}\}+\lambda f^2u[v_x]+\frac{1+f^2u^2}{u}[v_z]=N, \quad (5.7c)$$

$$\{\tilde{\rho}\}+\frac{f^2(2f-1)\lambda u}{f-1}[v_x]$$
$$+\frac{(f-1)(1+f^2u^2)+f^3u^2}{(f-1)u}[v_z]=f_E, \quad (5.7d)$$

$$\lambda fu[\tilde{\rho}]+f(1+2f^2\lambda^2u^2)[v_x]$$
$$+\lambda f(1+2f^2u^2)[v_z]-\frac{1}{s}[b_x]=f_x. \quad (5.7e)$$

Here, for an arbitrary function $F(z)$, we use the notation

$$[F]\equiv F(z=0^+)-F(z=0^-), \quad (5.8a)$$

$$\{F\}\equiv F(z=0^+)+F(z=0^-). \quad (5.8b)$$

[The junction conditions (5.7) can be obtained by applying the standard pillbox or integration loop method to the perturbation equations (5.5); or, equally well, they can be inferred from the nonlinear junction conditions (4.6)–(4.11) by linearization and by insertion of Eqs. (3.11), (3.15), and (3.16).] In the junction conditions (5.7) there appear several (normalized) delta-function sources of perturbations. Defined in terms of quantities evaluated at $z=0$, these sources are the following: N is the fractional perturbation of the rate of rest mass injection

$$N\equiv\delta\dot{M}/\rho\gamma u; \quad (5.9)$$

f_E is the fractional perturbation of the rate of injection of kinetic energy

$$f_E\equiv\delta\dot{E}_K/\rho\gamma u(f-1); \quad (5.10)$$

and f_x is the perturbation of the rate of injection of x component of momentum (i.e., the force in the x direction exerted on the magnetosphere by the perturbations of the injection process), divided by the rate of injection of rest mass

$$f_x\equiv\delta\dot{P}/\rho\gamma u. \quad (5.11)$$

B. Fourier-analyzed perturbation equations and junction conditions

Because both our stationary background and the background flow are symmetrical in time and in the x direction ($\partial/\partial t$ and $\partial/\partial x$ are two Killing vector fields), we can Fourier-analyze the magnetospheric perturbations in t and x without loss of generality; i.e., we can restrict attention to perturbations with sinusoidal dependences of t and x: $e^{-i(\omega t-k_xx)}$ for all perturbation quantities. Moreover, because of the constraint (5.6c), Eqs. (5.6a) and (5.6b) are not independent. In the following, we choose to eliminate b_x and use the resulting Eqs. (5.13a)–(5.13d) below as our *independent* MHD perturbation equations. We eliminate b_x and $b_{x,z}$ from these perturbation equations by means of

$$b_x=\frac{1}{u}\left[v_x-\lambda v_z-\left(\frac{\omega}{k_x}+\beta-V\right)b_z\right], \quad (5.12)$$

which is a combination of the Fourier-analyzed equations (5.6a) and (5.6c). By substituting (5.12) into (5.6b), and (5.6d)–(5.6f), our Fourier-analyzed MHD equations take the following form:

$$b_z' = ik_x(\lambda v_z - v_x) + i(\omega + \beta k_x - V)b_z, \tag{5.13a}$$

$$\left[\rho\gamma^2(1+\gamma^2V^2) - \frac{B^2}{4\pi}\right]uv_x' + \left[\rho\gamma^4 uV + \frac{\lambda B^2}{4\pi}\right]uv_z'$$
$$- \frac{B^2}{2\pi}uVb_z' - \frac{B^2}{4\pi}(1-u^2)\left\{\left[\frac{v_x-\lambda v_z}{u}\right]' - \left[\left[\frac{\omega}{k_x}+\beta-V\right]\frac{b_z}{u}\right]'\right\}$$
$$= -\frac{B^2}{4\pi}u'\left[v_x - \lambda v_z - \left[\frac{\omega}{k_x}+\beta-V\right]b_z\right] + \frac{B^2}{4\pi}[\lambda' + u(V-\beta)']b_z - ik_x\frac{B^2}{4\pi}(1-V^2)b_z$$
$$-\rho\gamma^2 u[(1+\gamma^2V^2)V' + \gamma^2 uVu']\tilde{\rho} - \rho\gamma^4 u[(1+4\gamma^2V^2)uu' + 4(1+\gamma^2V^2)VV']v_x$$
$$- \left[\frac{B^2}{4\pi}u\lambda' + \rho\gamma^2[(1+2\gamma^2u^2)(1+2\gamma^2V^2) - \gamma^2V^2]V' + 2\rho\gamma^4(1+2\gamma^2u^2)uVu'\right]v_z$$
$$+ i(\omega+\beta k_x)\left[\frac{B^2}{4\pi} + \rho\gamma^2(1+\gamma^2V^2)\right]v_x + i(\omega+\beta k_x)\left[\rho\gamma^4 uV - \frac{\lambda B^2}{4\pi}\right]v_z$$
$$- ik_x\left[\rho\gamma^2(1+\gamma^2V^2) - \frac{B^2}{4\pi}\right]Vv_x - ik_x\left[\rho\gamma^4 uV + \frac{\lambda B^2}{4\pi}\right]Vv_z, \tag{5.13b}$$

$$\left[\rho\gamma^2(1+\gamma^2u^2) - \frac{\lambda^2B^2}{4\pi}\right]uv_z' + \left[\rho\gamma^4 uV + \frac{\lambda B^2}{4\pi}\right]uv_x'$$
$$+ \frac{\lambda B^2}{2\pi}uVb_z' + \frac{\lambda B^2}{4\pi}(1-u^2)\left\{\left[\frac{v_x-\lambda v_z}{u}\right]' - \left[\left[\frac{\omega}{k_x}+\beta-V\right]\frac{b_z}{u}\right]'\right\}$$
$$= -\frac{B^2}{4\pi}(\lambda' - \lambda uu')\left\{\left[\frac{v_x-\lambda v_z}{u}\right] - \left[\left[\frac{\omega}{k_x}+\beta-V\right]\frac{b_z}{u}\right]\right\} - \frac{\lambda B^2}{4\pi}u(V-\beta)'b_z - ik_x\frac{B^2}{4\pi}(1-V^2)b_z$$
$$-\rho\gamma^2[(1+\gamma^2u^2)uu' + \gamma^2u^2VV' - V\beta']\tilde{\rho}$$
$$-\rho\gamma^2[\gamma^2u^2(1+4\gamma^2V^2)V' - (1+2\gamma^2V^2)\beta' + 2\gamma^2uV(1+2\gamma^2u^2)u']v_x$$
$$- \left[\rho\gamma^2(1+\gamma^2u^2)(1+4\gamma^2u^2)u' + 2\rho\gamma^4(1+2\gamma^2u^2)uVV' - 2\rho\gamma^4uV\beta' - \frac{\lambda B^2}{4\pi}u\lambda'\right]v_z$$
$$+ i(\omega+\beta k_x)\left[\frac{\lambda^2B^2}{4\pi} + \rho\gamma^2(1+\gamma^2V^2)\right]v_z + i(\omega+\beta k_x)\left[\rho\gamma^4uV - \frac{\lambda B^2}{4\pi}\right]v_x$$
$$- ik_x\left[\rho\gamma^2(1+\gamma^2u^2) - \frac{\lambda^2B^2}{4\pi}\right]Vv_z - ik_x\left[\rho\gamma^4uV + \frac{\lambda B^2}{4\pi}\right]Vv_x, \tag{5.13c}$$

$$u\tilde{\rho}' + (1+\gamma^2u^2)v_z' = -\gamma^2u[(1+\gamma^2V^2)V' + 2\gamma^2uVu']v_x + [(1-2\gamma^2u^2)(1+\gamma^2u^2)u'/u - 2\gamma^4u^2VV']v_z$$
$$+ i(\omega+\beta k_x - k_xV)\tilde{\rho} - i(\omega+\beta k_x)\gamma^2(Vv_x + uv_z) - ik_x(1+\gamma^2V^2+\gamma^2uV)v_x - ik_x\gamma^2uVv_z. \tag{5.13d}$$

(Here a prime denotes derivatives with respect to z. Note that this is the only kind of derivative present, since all stationary and Fourier-analyzed perturbation quantities depend only on the z coordinate.) The accompanying junction conditions [Eqs. (5.7a)–(5.7e)], in this sinusoidal situation and by virtue of Eq. (5.12), take the form

$$[b_z] = 0, \tag{5.14a}$$

$$\{\tilde{\rho}\} + \lambda f^2 u[v_x] + \frac{1+f^2u^2}{u}[v_z] = N, \tag{5.14b}$$

$$\{\tilde{\rho}\} + \frac{f^2(2f-1)\lambda u}{f-1}[v_x] + \frac{(f-1)(1+f^2u^2)+f^3u^2}{(f-1)u} \times [v_z] = f_E, \tag{5.14c}$$

$$\lambda fu[\tilde{\rho}] + f(1+2f^2\lambda^2u^2)[v_x] + \lambda f(1+2f^2u^2)[v_z]$$
$$- \frac{1}{su}\{v_x\} + \frac{\lambda}{su}\{v_z\} - \frac{2}{su}\left[\frac{\omega}{k_x} - V_F\right]b_z = f_x. \tag{5.14d}$$

To recapitulate, we will study the MHD perturbations on background flows having reflection symmetries

(4.1)–(4.3); the perturbations will be characterized by dimensionless quantities $\mathbf{v}$, $\mathbf{b}$, and $\tilde{\rho}$ [Eqs. (5.1)–(5.3)]; the MHD equations describing the time-dependent perturbations are Eqs. (5.5) or (5.6), together with a set of junction conditions [Eqs. (5.7a)–(5.7e)]; and the Fourier-analyzed perturbations are described by Eqs. (5.13a)–(5.13d), together with the Fourier-analyzed junction conditions (5.14a)–(5.14d).

C. General solution of the perturbation equations at infinity

In the regions $z \gg 1$ and $z \ll -1$, where the background functions β, u, V, and λ are constant (independent of z), the Fourier-analyzed MHD equations (5.13) can be solved analytically. These analytic solutions have been used to check the numerical code described in the next section; they also are useful in understanding the results of the numerical calculations, since the numerical solutions must asymptote to them at large $|z|$. These analytic solutions also exhibit explicitly the effects of β (i.e., of transforming to coordinates that slide with velocity $dx/dt=-\beta$) on the perturbation modes.

It is very tedious though maybe straightforward to derive the analytic solutions directly from the perturbation equations (5.13); and we did not do so. Rather, we derived them by first writing down the general solutions in the rest frame of the fluid, and by then performing a Lorentz boost to the FIDO's rest frame.

In the fluid's rest frame (denoted by primes) with a uniform magnetic field along the z' direction, and the velocity and the magnetic field restricted to the x'-z' plane, the Fourier components of the magnetosonic modes satisfy

$$v_x':v_z':b_x':b_z':\tilde{\rho}=1:0:\left[-\frac{k_z'}{\omega'}\right]:\left[\frac{k_x'}{\omega'}\right]:\left[\frac{k_x'}{\omega'}\right]; \tag{5.15}$$

and the frequency ω' and wave vector (k_x', k_z') are related by the dispersion relation

$$(\omega')^2=\frac{\mathbf{B}'^2}{4\pi\rho+\mathbf{B}'^2}[(k_x')^2+(k_z')^2] \ . \tag{5.16}$$

There are also two "convective modes" (zero-temperature limit of the slow magnetosonic modes) that have zero frequency in the fluid's frame:

$$\mathbf{b}'=v_x'=0, \quad v_z' \text{ arbitrary function of } x', z' \ , \qquad \tilde{\rho}=-t'\nabla'\cdot\mathbf{v}' \ ; \tag{5.17}$$

and

$$\mathbf{v}'=\mathbf{b}'=0, \quad \tilde{\rho} \text{ arbitrary function of } x', z'. \tag{5.18}$$

The Lorentz boost from the fluid's rest frame to the FIDO's rest frame, in 3+1 form with the fluid-frame quantities expressed in terms of the FIDO-frame quantities, has the following form (see, for example, Jackson[26]):

$$\mathbf{B}'=\frac{\mathbf{B}}{\gamma}+\frac{\gamma\mathbf{B}\cdot\mathbf{V}}{\gamma+1}\mathbf{V} \ , \tag{5.19a}$$

$$\delta\mathbf{B}'=\frac{\delta\mathbf{B}}{\gamma}+\gamma(\mathbf{B}\cdot\nabla\mathbf{v}-\mathbf{V}\cdot\nabla\mathbf{B})+\frac{\gamma\delta\mathbf{B}\cdot\mathbf{V}}{\gamma+1}\mathbf{V} \ , \tag{5.19b}$$

$$\mathbf{v}'=\frac{\gamma^3\mathbf{V}}{\gamma+1}\mathbf{V}\cdot\mathbf{v}+\gamma\mathbf{v} \ , \tag{5.19c}$$

$$\omega'=\gamma(\omega+\beta k_x-k_xV-k_zu) \ , \tag{5.19d}$$

$$\mathbf{k}'=\mathbf{k}-\left[\omega+\beta k_x-\frac{\gamma}{\gamma+1}(k_xV+k_zu)\right]\mathbf{V} \ . \tag{5.19e}$$

This boost brings the fluid-frame MHD solutions into the following FIDO-frame form: For the fast magnetosonic modes, the solution [Eq. (5.15)] becomes

$$b_x=-\frac{(1+\lambda^2-C^2)k_z}{\omega+\beta k_x-k_xV-k_zu}Ae^{-i(\omega t-k_xx-k_zz)}, \tag{5.20a}$$

$$b_z=\frac{(1+\lambda^2-C^2)k_x}{\omega+\beta k_x-k_xV-k_zu}Ae^{-i(\omega t-k_xx-k_zz)}, \tag{5.20b}$$

$$v_x=(1-Cv)Ae^{-i(\omega t-k_xx-k_zz)}, \tag{5.20c}$$

$$v_z=(\lambda+Cu)Ae^{-i(\omega t-k_xx-k_zz)}, \tag{5.20d}$$

$$\tilde{\rho}=\frac{k_x-(\omega+\beta k_x)V-\lambda[k_z-(\omega+\beta k_x)u]}{\omega+\beta k_x-k_xV-k_zu}\times Ae^{-i(\omega t-k_xx-k_zz)}, \tag{5.20e}$$

where A is a constant wave amplitude. The dispersion relation (5.16) for these modes takes the following form:

$$(\omega+\beta k_x-k_xV-k_zu)^2-(1+\lambda^2-C^2)\frac{u}{s\gamma}\times[k_x^2+k_z^2-(\omega+\beta k_x)^2]=0. \tag{5.21}$$

The dispersion relation (5.21) can be regarded as a quadratic equation for k_z in terms of known quantities $(\omega, k_x, \ldots)$. For some ranges of ω and k_x there will be no real solutions; i.e., fast magnetosonic waves will not be able to propagate to infinity. For other ranges there will be two real solutions, one describing outward-propagating magnetosonic waves; the other, inward-propagating.

The two convective modes both have dispersion relations

$$\omega+\beta k_x-k_xV-k_zu=0 \tag{5.22}$$

corresponding to $\omega'=0$. One convective mode [Eq. (5.17)] involves frozen-in velocity perturbations, which can be thought of as put into the fluid at $z=0$. These velocity perturbations produce a density perturbation that grows linearly with time in the fluid frame, and linearly with z in the FIDO frame:

$$\mathbf{b}=0, \tag{5.23a}$$

$$v_x=\lambda Ae^{-i(\omega t-k_xx-k_zz)}, \tag{5.23b}$$

$$v_z=Ae^{-i(\omega t-k_xx-k_zz)}, \tag{5.23c}$$

$$\tilde{\rho}=i\frac{\lambda k_x+k_z}{\beta k_x-k_xV-k_zu}k_zzAe^{-i(\omega t-k_xx-k_zz)} \ . \tag{5.23d}$$

The other convective mode involves a frozen-in density perturbation and no velocity perturbation:

$$\mathbf{b}=0,\quad \mathbf{v}=0,\quad \tilde{\rho}=Ae^{-i(\omega t-k_x x-k_z z)}. \tag{5.24}$$

For the stationary "magnetosphere" of Sec. IV, the periodic perturbations at the interface $z=0$ will produce waves that propagate out to $|z|\gg 1$, where they become a mixture of above fast magnetosonic and "convective" modes.

VI. INTERACTION Of MHD WAVES WITH THE SHIFT FUNCTION: NUMERICAL RESULTS

In this section we shall present the results of our numerical solutions of the Fourier-analyzed MHD perturbation equations [Eqs. (5.13)]. These equations are ordinary differential equations (ODE's) with z as the independent variable. They have been solved in the stationary background of Sec. IV (Fig. 4 and related discussions), subject to the following boundary conditions at spatial infinity ($z\to\pm\infty$) and at the interface ($z=0$). At spatial infinity (numerically, very large $|z|$ where the background flow has constant values) we require that

there are no ingoing waves at both $z\to+\infty$ and $z\to-\infty$. (6.1)

At the interface, we require that [see also Eqs. (5.14a)–(5.14d)]

$$b_z^+=b_z^-\ , \tag{6.2a}$$

$$f_E^{\pm}=\tilde{\rho}^{\pm}\pm\frac{f^2(2f-1)\lambda u}{f-1}v_x^{\pm}\pm\frac{(f-1)(1+f^2u^2)+f^3u^2}{(f-1)u}v_z^{\pm}\ , \tag{6.2b}$$

$$N^{\pm}=\tilde{\rho}^{\pm}\pm\lambda f^2 u v_x^{\pm}\pm\frac{1+f^2u^2}{u}v_z^{\pm}\ , \tag{6.2c}$$

$$f_x=\lambda f u[\tilde{\rho}]+f(1+2f^2\lambda^2u^2)[v_x]+\lambda f(1+2f^2u^2)[v_z]-\frac{1}{su}\{v_x\}+\frac{\lambda}{su}\{v_z\}-\frac{2}{su}\left[\frac{\omega}{k_x}-V_F\right]b_z. \tag{6.2d}$$

Here, $f_E^{\pm}$, $N^{\pm}$, and f_x are dimensionless perturbations to the stationary delta-function sources of kinetic energy, rest mass, and x momentum at the interface, with frequency ω, and wave number k_x; see Sec. V, Eqs. (5.9)–(5.11). What we shall study are MHD perturbations that are driven at $z=0$ by $f_E^{\pm}$, $N^{\pm}$, and f_x and propagate toward $z=\pm\infty$. We shall study how these perturbations interact with the shift function and the stationary background flow as they propagate.

Each perturbation solution has specific values of ω and k_x; i.e., it can be thought of as lying at a particular point in the ω-k_x plane. We have restricted our numerical calculation to those regions of the ω-k_x plane where (i) $\omega>0$ (an arbitrary convention), (ii) $k_x>0$ (this is the only region in which superradiance can occur for our model spacetime), and (iii) all k_z's are real at $z\to\pm\infty$, i.e., (outgoing) fast magnetosonic waves can propagate at both $z\to\infty$ and $z\to-\infty$. By imposing (iii) above in the dispersion relation (5.21), we infer that the boundaries of this region are also, besides $\omega=0$ and $k_x=0$,

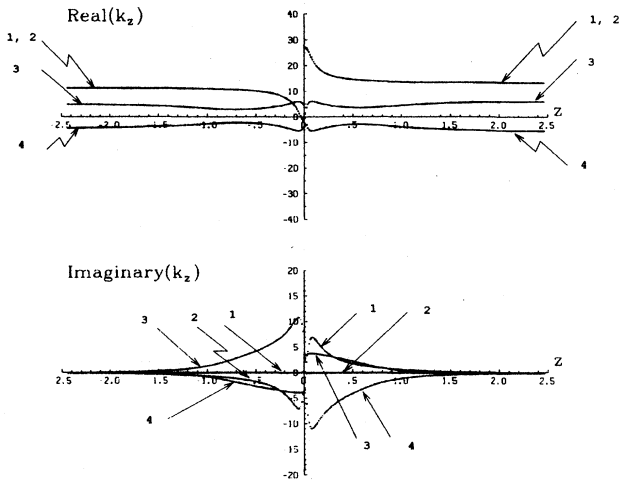

FIG. 4. Local wave numbers k_z of MHD perturbations as functions of z for the stationary background shown in Fig. 3. The perturbations have frequency $\omega=6.5$ and wave number $k_x=3$.

$$\omega=-\beta(z)k_x+\frac{V}{1-u^2+\frac{u}{s\gamma}(1+\lambda^2-C^2)}k_x\pm\frac{k_x}{1-u^2+\frac{u}{s\gamma}(1+\lambda^2-C^2)}\times\left[V^2-u^2+\frac{u}{s\gamma}(1+\lambda^2-C^2)+u^2\left[u-\frac{1}{s\gamma}(1+\lambda^2-C^2)\right]^2\right]^{1/2}. \tag{6.3}$$

For our chosen stationary background,

$$u(\pm\infty)=\pm0.49\ ,\quad V(\pm\infty)=\pm0.06\ ,$$
$$\gamma(\pm\infty)=1.15\ ,\quad \lambda(\pm\infty)=-3.99\ ,$$
$$C(+\infty)=2.0\ ,\quad C(-\infty)=-2.0\ ,$$
$$\beta(+\infty)=0\ ,\quad \beta(-\infty)=-4.0\ ,$$

these boundaries are $\omega=0$, $\omega=4.99k_x$, $\omega=3.01k_x$, $\omega=0.99k_x$, and $k_x=0$. By examining the dispersion relation (5.21) more closely, we can identify that

$$\omega\geq 0.99k_x$$

corresponds to k_z real at $z=+\infty$; and

$$\omega\geq 4.99k_x$$

or

$$\omega\leq 3.01k_x$$

corresponds to k_z real at $z=-\infty$. Therefore, if we re-

strict attention to $0.01 \le \omega \le 9.99$, then

$$\begin{aligned} &0.01 \le 0.99k_x \le \omega \le 3.01k_x \ , \\ &4.99k_x \le \omega \ \le 9.99 \end{aligned} \tag{6.4}$$

are the regions of the ω-k_x plane that we shall study.

For each point in the ω-k_x region (6.4), there are five independent solutions with outgoing waves at $z \to \pm\infty$, corresponding to five independent values of the sources $f_E^{\pm}$, $N^{\pm}$, f_x. These five solutions have been constructed by the following procedure. (i) Integrate the ODE's (5.13) outward from $z=0$ to $z=+\infty$ starting, in turn, with only one of b_z, v_x, v_z, $\tilde{\rho}$ nonzero; thereby obtain four independent solutions at $z>0$. (ii) Similarly integrate (5.13) from $z=0$ to $z=-\infty$ starting, in turn, with only one of b_z, v_x, v_z, $\tilde{\rho}$ nonzero; thereby obtain four independent solutions at $z<0$. (iii) For each of the five choices of $\{f_E^{\pm}, N^{\pm}, f_x\}$, impose the eight boundary conditions (6.1), (6.2) on the eight numerical solutions (four at $z>0$, four at $z<0$) to get a unique solution that satisfies the ODE's and the boundary conditions.

The ODE's (5.13) comprise a coupled fourth-order ODE system. For most choices of ω, k_x this system is stiff near the interface; i.e., there is one heavily damped solution and three growing solutions. This stiffness can be quantified as follows: at a fixed z, write the ODE's (5.13) in the form

$$y_i' = Q_i^j y_j \ , \tag{6.5}$$

where $y_1=b_z$, $y_2=v_x$, $y_3=v_z$, $y_4=\tilde{\rho}$. Then the matrix Q_i^j (at fixed z) has four eigenvectors

$$Y_i = A_i^j y_j \tag{6.6a}$$

and four corresponding eigenvalues $k_{z,i}$; i.e.,

$$Y_i' = k_{z,i} Y_i \quad \text{(no summation)}. \tag{6.6b}$$

These Y_i's are locally sinusoidal solutions with local wave numbers $k_{z,i}$. Shown in Fig. 4 are the four local wave numbers $k_{z,i}$ as functions of height z for a typical set of (ω, k_x). [Note the near-degeneracy even at $|z| \ll 1$ of two of the eigenvalues, which asymptote to the degenerate convective modes (5.23), (5.24) at $|z| \gg 1$.] At large $|z|$, these $k_{z,i}$'s are all constant, and therefore the locally sinusoidal solutions are globally (at $|z| \gg 1$) sinusoidal. At $|z| \ll 1$, the imaginary parts of the local k_z's are usually big, and the real parts change rapidly with z. One of the four $\mathrm{Im}(k_z)$'s is positive for $z>0$ and one is negative for $z<0$; this is the strongly damped solution, which produces the stiffness of the equations. A numerical solution to the ODE's, starting from a given value at $z=0$, will be altered strongly, because of the large and rapidly changing $k_{z,i}$'s, as it tries to propagate to the uniform region ($z=\pm\infty$). The imaginary part of k_z is produced by β', the spatial derivative of the shift function and the spatial derivatives of MHD variables—which are also caused by β'. Therefore, starting from a given initial condition at $z=0$, how the numerical solution evolves to its sinusoidal form at large $|z|$, and what sinusoidal form the solution evolves to are completely determined by β', once the frequency ω and the wave number k_x are fixed.

The ODE system (5.13) for our Fourier analyzed MHD perturbations has been solved using the well-known ODE solver, the LSODE package.[27] This is a variable-step, variable-order code using linear multistep methods. For stiff systems such as ours, it uses backward differentiation formulas (BDF) with maximum order 5. To ensure the correct coding of our MHD perturbation equations [Eqs. (5.13)], we have used the symbolic manipulating program (SMP) (Ref. 28) to eliminate algebraic coding errors. We have also checked our numerical solutions in the uniform region against the analytic solutions presented in Sec. V [Eqs. (5.20)–(5.24)]. In the nonuniform region, we have spot-checked the code to be sure that the numerical solutions satisfy the first-order perturbed differential-energy-conservation law. Details of our numerical methods and checks, and of the numerical accuracy, are discussed in the Appendix.

In Fig. 5 is shown a typical one of our numerical solutions. This solution has $\omega=6.5$ and $k_x=3.25$, and its driving "force" is $f_x=10^{-6}$, $f_E^+=f_E^-=N^+=N^-=0$. Notice this solution's rapid, nonsinusoidal changes near $z=0$, and the manner in which it finally settles down to a sinusoidal form in the region $|z| \gg 1$. By studying how these perturbations settle into their asymptotic forms and what asymptotic forms they settle into, we shall be able to infer the effects of the shift function on the MHD perturbations. By studying perturbations at different frequency ω and wave number k_x, we will be able to infer the response of the MHD system to perturbations in the ω-k_x plane.

As an aid to understanding our perturbation solutions, we shall mostly examine the perturbation variables $\mathbf{v}$, $\mathbf{b}$,

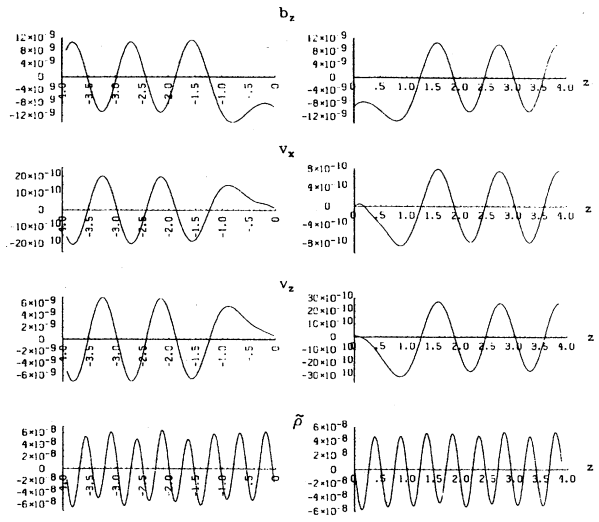

FIG. 5. A typical numerical solution of MHD perturbation equations (5.13). Only the four independent perturbation variables b_z, v_x, v_z, $\tilde{\rho}$ are plotted. The perturbations are excited by $f_x=10^{-6}$ alone at the interface $z=0$ (i.e., $f_E^{\pm}=N^{\pm}=0$), and there are no ingoing waves at large $|z|$. The perturbations in the MHD background flow interact with the background strongly near $z=0$, and do not have a simple wave form. At large $|z|$, the perturbations are a superposition of outgoing sinusoidal waves.

and $\tilde{\rho}$, but also the z component of the first-order perturbation of the energy flux as measured by FIDO's. The exact, nonlinear energy flux measured by the FIDO's is

$$\mathbf{S}=\rho\gamma^2\mathbf{V}+\frac{1}{4\pi}(\mathbf{V}\times\mathbf{B})\times\mathbf{B}\ ; \tag{6.7}$$

and the first-order perturbation of its z component is

$$\delta S^z=\rho\gamma u[\tilde{\rho}\gamma+2\gamma^3(Vv_x+uv_z)+\gamma v_z/u -\lambda(Vb_z-ub_x-\lambda v_z+v_x)/s-Cb_x/s]\ . \tag{6.8}$$

This first-order energy flux is a modulation of the stationary flux and has zero time-averaged value. A nonzero time-averaged energy flux carried by the perturbations shows up only at second (quadratic) order. This second-order flux will not be of interest to us: We wish to understand the modulation of the outpouring energy by the perturbations; and the modulation is embedded in the first order δS_z.

In the following, we shall describe our solutions for the outflowing waves generated by various delta-function sources in terms of the following quantities: (i) the perturbations b_z, v_x, v_z, $\tilde{\rho}$ excited at the interface; (ii) the ratios of the asymptotic values of b_z, v_x, v_z, $\tilde{\rho}$ to their values at the interface; (iii) the ratio of the first-order energy flux δS_z evaluated at $z\to\pm\infty$ to that at the interface. These quantities will be plotted as functions of frequency ω at fixed wave number k_x, functions of wave number k_x at fixed frequency ω, and functions of (ω, k_x) in three-dimensional plots. The ratios of quantities at $z=\pm\infty$ to those at $z=0$ reflect how strongly (the curl of) the shift function interacts with the MHD perturbations; and the size of the perturbation variables at the interface represents how easily a perturbation to the stationary flow can be excited by the "driving force" at the interface. Variations of these quantities in the ω-k_x plane characterize the response of our MHD system to the "driving force" at different frequencies ω and wave numbers k_x. This study will give us insight into understanding some general features of interactions of MHD perturbations with the shift function, and will help us to identify some interesting directions for future research.

Shown in Figs. 6–8 are perturbations on both sides of the interface excited by three types of delta-function sources: $\{f_x=10^{-6},\ f_E^{\pm}=N^{\pm}=0\}$, $\{f_E^{+}=f_E^{-}=10^{-6},\ f_x=N^{\pm}=0\}$, and $\{N^{+}=N^{-}=10^{-6},\ f_x=f_E^{\pm}=0\}$. Shown in Figs. 9–12 are the ratios of the first-order FIDO-measured energy fluxes evaluated at $z=\pm7.35$ and $z=0$, at fixed frequency $\omega=6.5$ or as functions of ω and k_x. (Since the length scale of the background is ~1, $z=\pm7.35$ is far enough into the uniform region to be representative of conditions at $z=\pm\infty$. See Figs. 3–5.) In the three-dimensional plots, the vertical direction represents the quantities being plotted, and the flat floor is the region outside (6.4), where we have not constructed solutions.

In these figures, we see four distinct classes of responses in the ω-k_x plane. There are resonance near the line

$$\omega+\beta(0)k_x\equiv\omega-V_Fk_x=0\ , \tag{6.9}$$

which manifest themselves as ridges or neighboring ridges and valleys; there are ridges along lines parallel to (6.9); there are undulations along lines parallel to (6.7); and there are single shallow valleys along (6.9). All these appear only in the "superradiant" region, the region in

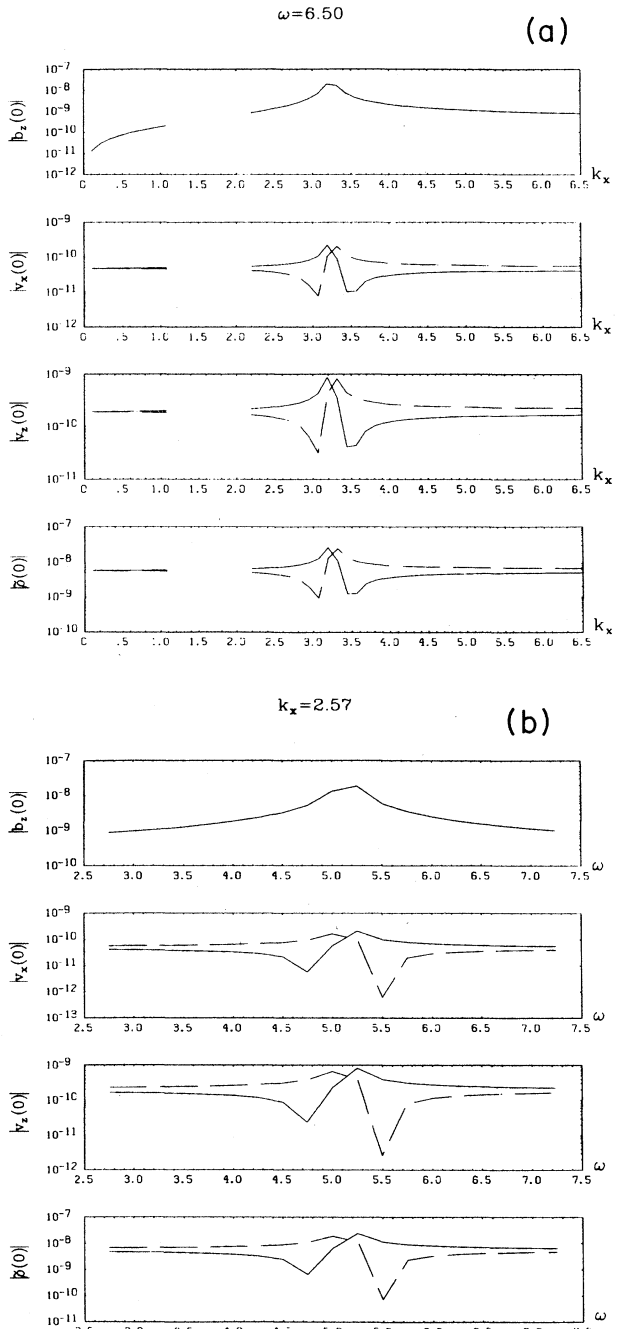

FIG. 6. Perturbations excited by $f_x=10^{-6}$ alone (i.e., $f_E^{\pm}=N^{\pm}=0$) at the interface. Note the resonance at $\omega+\beta(0)k_x=0$ [$\beta(0)=-2$]. Solid curves represent perturbations excited on the positive z side of the interface. Dashed curves represent perturbations on the negative side of the interface. (a) perturbations at fixed frequency $\omega=6.5$; (b) perturbations at fixed wave number $k_x=2.57$.

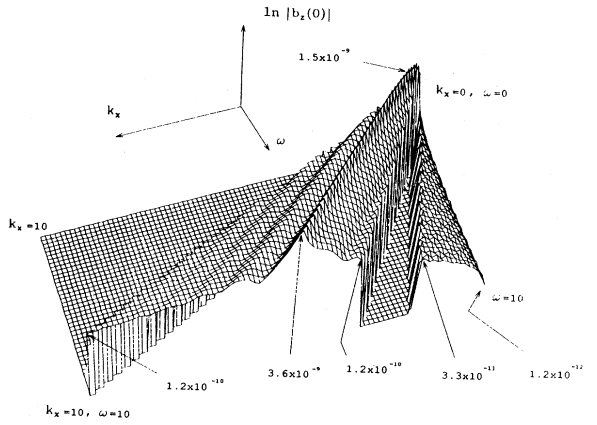

FIG. 7. Perturbations to the magnetic field b_z excited on both sides of the interface by a delta-function source $f_E^+ = f_E^- = 10^{-6}$ alone at the interface. Perturbations to the fluid variables do not show much variation and thus are not given here.

the ω-k_x plane where the FIDO-measured wave frequency

$$\omega_0 \equiv \omega + \beta(z) k_x \tag{6.10}$$

has opposite signs for FIDO's at $z \to -\infty$ from those at $z \to \infty$. We have seen no distinctive features in that part of the nonsuperradiant region which we have explored: $0 < 4.99 k_x \leq \omega \leq 9.99$.

Of these features, the most interesting seems to be the resonance along $\omega - V_F k_x = 0$. The key feature of $\omega - V_F k_x$ is not its role as the FIDO-measured angular frequency at the interface, but rather its role as the angular frequency in the field lines' rest frame at the point $z = 0$, where the driving "forces" act. We shall emphasize this by denoting $\omega - V_F k_x \equiv \omega_F$ (F for "field lines"). *The resonance occurs, then, at $\omega_F = 0$, i.e., for*

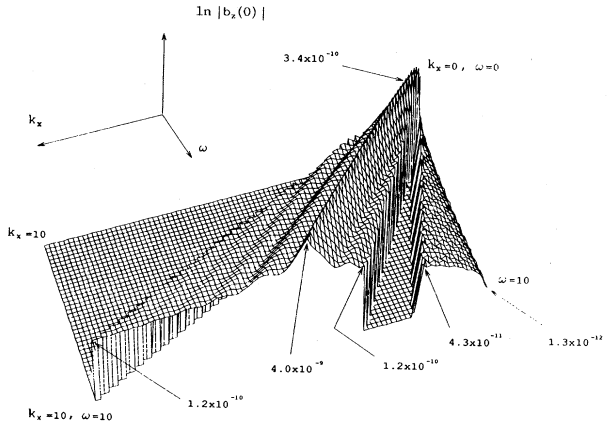

FIG. 8. Perturbations to the magnetic field b_z excited on both sides of the interface by a delta-function source $N^+ = N^- = 10^{-6}$ alone at the interface. Perturbations to the fluid variables do not show much variation and thus are not given here.

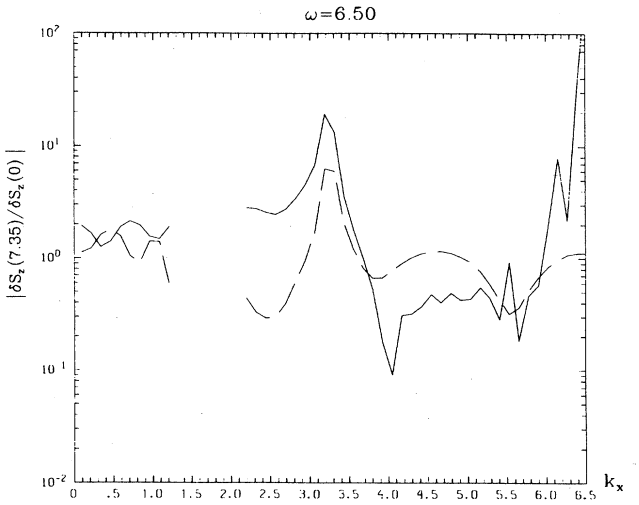

FIG. 9. The ratio $|\delta S_z(\pm 7.35)/\delta S_z(0)|$ for perturbations excited by $f_x = 10^{-6}$ alone at the interface $z = 0$. Here $\delta S_z(z)$ is the first-order perturbation of the z component of the FIDO-measured energy flux [Eq. (6.6)]. The region where curves break is the region where MHD waves cannot propagate freely at $z \to -\infty$ and where numerical computations have not been done. Solid curves correspond to perturbations on the $z > 0$ side; dashed curves correspond to perturbations on the $z < 0$ side. The perturbations are excited at the fixed frequency $\omega = 6.5$.

those values of ω and k_x, which produce vanishing angular velocity in the field lines' rest frame at the point where the driving "forces" act. Evidently, it is easier to drive perturbations, with a fixed rate of injection of linear momentum $f_x \rho \gamma u$ or a fixed rate of injection of kinetic energy $f_E \rho \gamma u (f - 1)$, when one does so near zero frequency in the field's rest frame, $\omega_F \simeq 0$, than when one does so well away from zero frequency, $|\omega_F| \gtrsim 1$. As Fig. 13 shows for $|v_x(-7.35)/v_x(0)|$ not only are the perturbation quantities b_z, v_x, v_z, and $\tilde{\rho}$ especially easily excited at $\omega_F \simeq 0$, it is also especially easy for these perturbations to propagate to $z = \infty$, carrying with them a modulation of the magnetosphere's outflowing energy.

The case of injection of linear momentum corresponds most closely to buffeting of a black-hole magnetosphere, in the plasma-creation region, by lumpy accretion-disk **B** fields. For this case the strength of the driving force can be characterized by its amplitude of injected momentum per unit area, i.e., the amplitude $\delta T_{xz} = \rho \gamma u f_x$ of the oscillatory discontinuity in the stress. When divided by the equilibrium magnetosphere's conserved stress $T_{xz} = \rho \gamma u l$ [see Eqs. (3.28) and (3.30′) of Ref. 19], this injected momentum-per-unit area gives a dimensionless driving force

$$\frac{\delta T_{xz}}{T_{xz}} = \frac{f_x}{l} = \frac{f_x}{40} \tag{6.11}$$

that is a better measure of the strength of the force than f_x alone. Here, $l = 40$ is the value of l used throughout

our numerical calculations. Since our numerical calculations also use $f_x = 10^{-6}$, the value of this dimensionless driving force is $\delta T_{xz}/T_{xz} = 2.5 \times 10^{-8}$. This driving force produces a magnetospheric response in the plasma production plane, which can be characterized by the amplitude $\delta S_x(z=0)$ of the modulations of the FIDO-measured upward energy flux. From Fig. 14 we read off the value $\delta S_z(z=0) \simeq 2.9 \times 10^{-8} \rho\gamma u$. For comparison, in the unperturbed magnetosphere the upward energy flux at $z=0$ is $S_z = \rho\gamma u f = 1.01 \rho\gamma u$ [see Eqs. (3.28) and (3.31') of Ref. 19]. By combining these numbers with Eq. (6.11), we obtain

$$\frac{\delta S_z(z=0)}{S_z(z=0)} \simeq 1.15 \frac{\delta T_{xz}}{T_{xz}} . \tag{6.12}$$

In words: the driving force produces a fractional modulation of the magnetosphere's energy flux, at $z=0$ and on

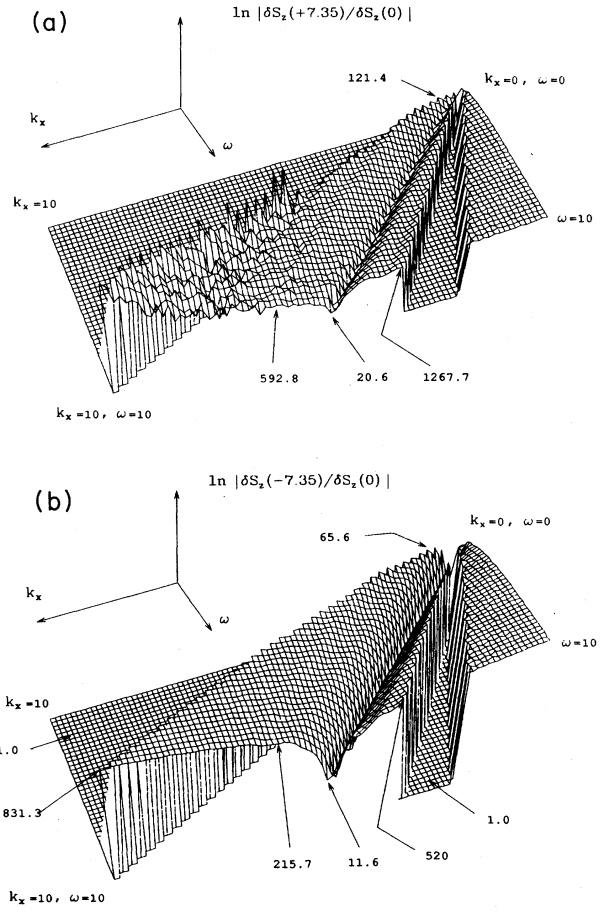

FIG. 10. The ratio $|\delta S_z(\pm 7.35)/\delta S_z(0)|$ for perturbations excited by $f_x = 10^{-6}$ alone at the interface $z=0$. Here the ratio is plotted in the logarithmic scale. The flat floor is the region where MHD waves cannot propagate freely at $z \to -\infty$ and where the computation is not done. They have been assigned value one in these three-dimensional plots. (a) The ratio $|\delta S_z(7.35)/\delta S_z(0)|$ for perturbations on the $z>0$ side; (b) the ratio $|\delta S_z(-7.35)/\delta S_z(0)|$ for perturbations on the $z<0$ side.

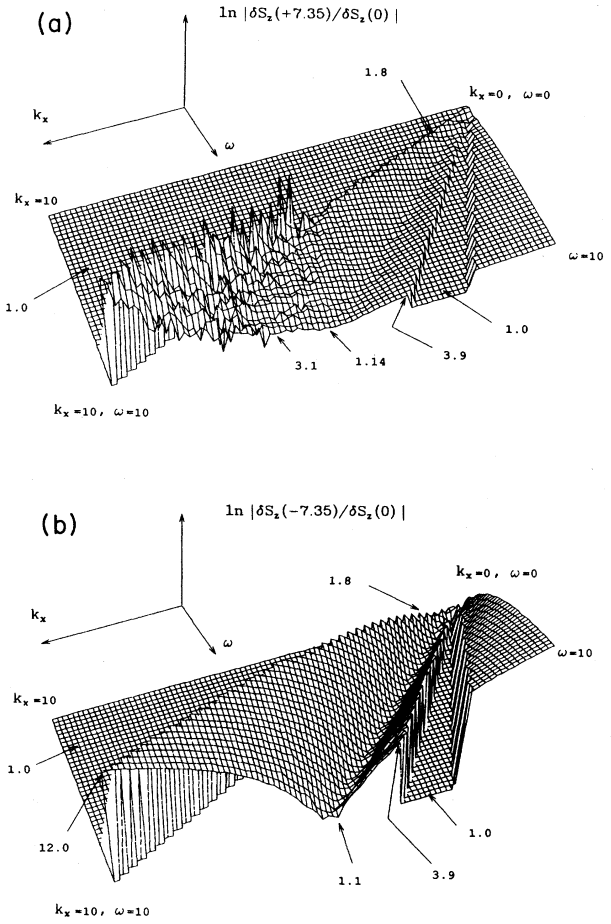

FIG. 11. Same quantities as plotted in Fig. 10, but for perturbations excited by $f_E^+ = f_E^- = 10^{-6}$ alone at the interface.

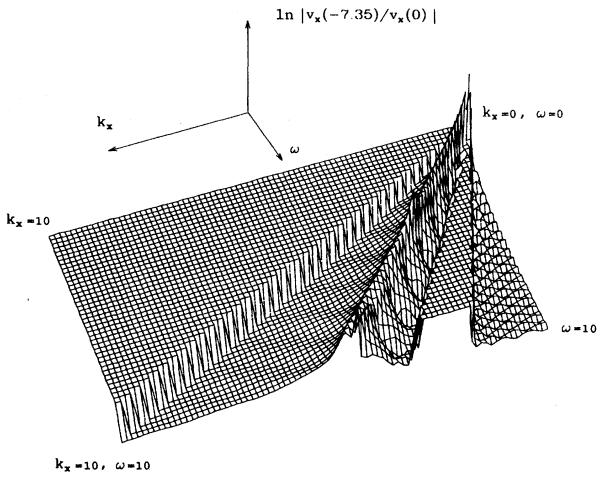

FIG. 12. Same quantities as plotted in Fig. 10, but for perturbations excited by $N^+ = N^- = 10^{-6}$ alone at the interface.

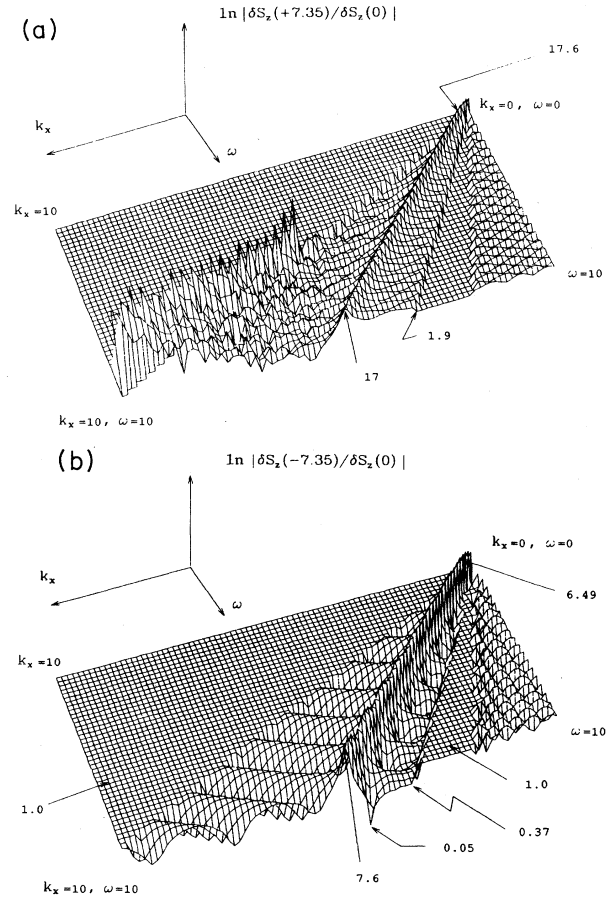

FIG. 13. Amplification factor for v_x (ratios of amplitudes of perturbations evaluated at large $|z|$ and at $z=0$) for perturbations excited by $f_x=10^{-6}$ alone at $z=0$. Here the ratio is plotted in the logarithmic scale. The flat floor is the region where MHD waves cannot propagate freely at $z\to-\infty$. Note the undulation in $|v_x(-7.35)/v_x(0)|$.

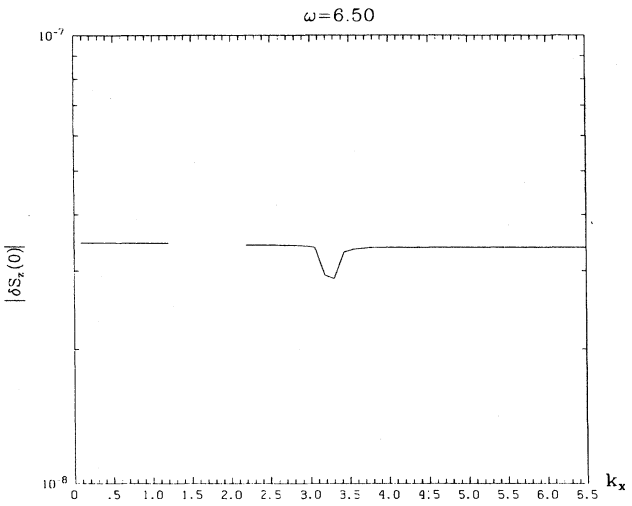

FIG. 14. Energy flux at the interface, excited by $f_x=10^{-6}$ at $z=0$ alone. Note that when excited by only f_x, $\delta S_z(0)$ is continuous at the interface.

resonance, that is nearly the same as the dimensionless measure $\delta T_{xz}/T_{xz}$ of the force.

As the magnetospheric perturbations propagate outward to $z\gg1$, they get amplified by an amount (Fig. 9)

$$\frac{\delta S_z(z\gg1)}{\delta S_z(z=0)}\simeq 19\ , \tag{6.13}$$

on resonance. Off resonance, this "amplification factor" is usually in the range 0.2–3. For comparison, the amplification of the upward energy flux in the unperturbed magnetosphere is, since $S_z=\rho\gamma u(f+Cl)$ at all heights,

$$\frac{S_z(z\gg1)}{S_z(z=0)}=\frac{f+V_F l}{f}\simeq 80\ ; \tag{6.14}$$

this is 4 times larger than the amplification (6.13) of the perturbation. By combining Eqs. (6.12) and (6.14) we see that on resonance the fractional modulation of the distant wind's energy flux is about one-third the dimensionless measure of the driving force:

$$\frac{\delta S_z(z\gg1)}{S_z(z\gg1)}\simeq 0.3\frac{\delta T_{xz}}{T_{xz}}\ . \tag{6.15}$$

Thus, the wind's response on resonance is strong, but not terribly strong.

VII. IMPLICATIONS FOR KERR BLACK HOLES

In the numerical results presented in Sec. VI we saw resonances near $\omega_F\equiv\omega-V_F k_x=0$ in the ω-k_x plane—i.e., for values of ω and k_x that produce a near-vanishing angular frequency in the rest frame of the field lines in the driving region. It is reasonable to speculate that a similar behavior will occur in the magnetosphere of a Kerr black hole.

In the magnetosphere of a Kerr hole the field-line angular velocities Ω_F are constant along each field line, but may differ from one field line to another. However, from detailed studies of magnetospheres,[5,11,12] it seems likely that the variations are not great and that Ω_F is approximately equal to one-half the angular velocity of rotation of the hole's horizon, $\Omega_F\simeq\Omega_H/2$.

For a Kerr hole the angular quantum number m (which takes on integral values) is the analog of our planar magnetosphere's k_x, and the perturbation angular frequency ω as measured at infinity is the analog of our planar ω. The perturbation angular frequency ω_F as measured at any radius in the rest frame of the field lines (but using as the "clock" the "universal time" t of the membrane paradigm—i.e., the Killing-vector defined time t, i.e., the Boyer-Lindquist time coordinate t, i.e., proper time as measured at infinity) is given by $\omega_F=\omega-m\Omega_F$. This is the analog of our planar relation $\omega_F=\omega-k_x V_F$. Thus, if our planar results can be extrapolated to a Kerr black hole, then *perturbations of a Kerr hole's magnetosphere with angular quantum number m may be especially easy to excite at angular frequencies, as measured at infinity, given by*

$$\omega\simeq m\Omega_F\simeq\frac{m}{2}\Omega_H=\frac{m}{4M}\frac{a}{1+\sqrt{1-a^2}}\ . \tag{7.1}$$

Here, M is the hole's mass and a is its dimensionless angular momentum parameter (its angular momentum divided by its squared mass).

A likely driving force for perturbations of a Kerr hole is the Maxwell pressure of nonaxisymmetrically distributed magnetic field lines anchored in the innermost region of the accretion disk—i.e., chaotic clumps of field lines anchored in the disk. Such a clump will orbit the hole with an angular velocity approximately equal to the "Keplerian" (geodesic) angular velocity at the radius of the lump of plasma that anchors it; and as it orbits, its Maxwell pressure will buffet the field lines that thread the hole, thereby driving magnetospheric perturbations.

In order for such a clump of field lines to drive magnetospheric perturbations on resonance, the Keplerian angular velocity [e.g., Eq. (5.4.3) of Ref. 29]

$$\Omega_K = \frac{M^{1/2}}{r_L^{3/2} + aM^{3/2}} \tag{7.2}$$

of its anchoring lump (which orbits at radius r_L) must be approximately equal to the field-line angular velocity (7.1). This implies for a rapidly rotating hole $a \simeq 1$ that

$$r_L \simeq \frac{(4-m)^{2/3}}{m^{1/3}} M = (2.08,\ 1.26,\ 0.69)\ M \quad .$$

Here, 2.08 corresponds to $m=1$, 1.26 corresponds to $m=2$, and 0.69 corresponds to $m=3$. For an extreme Kerr black hole, the last stable circular orbit for a corotating particle is at $r=M$. Therefore, for a Keplerian orbit, only a very few angular quantum numbers can be responsible for this kind of resonant excitation. On the other hand, the disk's pressure gradient may well force clumps that are anchored near its inner edge to orbit at an angular velocity faster than Keplerian. In this case, resonant excitations can occur for more angular quantum numbers m than the Keplerian orbit would predict.

It is far from certain that the resonance seen at $\omega_F = 0$ in our planar magnetosphere will also show up in the magnetosphere of a Kerr hole. Only a detailed study of the dynamics of Kerr-hole magnetospheres can reveal for sure. If the resonance does show up and is much more easily excited than in our model magnetosphere [Eq. (6.15)], then observations of temporal modulations of the innermost regions of jets in active galactic nuclei might someday reveal the angular velocities of the central hole's magnetic field lines.

VIII. CONCLUSIONS AND FUTURE RESEARCH

The numerical calculations presented here have raised more questions than have been answered. However, they do point out some interesting directions for future research. Of those features we see in Sec. VI, the most striking is the resonance near $\omega_F \equiv \omega - V_F k_x = 0$. It would be useful to understand more deeply this resonance in terms of the structures of the gravitational and MHD background. To help us understand this resonance, it would also be useful to perform a more detailed calculation to locate the precise sites of this resonance in the ω-k_x plane (in particular, to determine if a finite flow speed at $z=0$ will shift the location of the resonance line). In Sec. VII we speculated about the implications of this resonance for the magnetosphere of a Kerr black hole. The need for perturbation computations in the Kerr geometry, or at the least in the planar model spacetime (2.3) with a horizon, is obvious. Even in the planar spacetime (2.4) of this paper, additional studies would be useful: Perturbations with $\delta B_y \neq 0$ would correspond more closely than those of this paper ($\delta B_y = 0$) to a Kerr magnetosphere perturbed by clumpy fields in a surrounding disk, and the influence of a nonzero y component of the wave vector deserves study.

We have also seen undulations in the ratios of energy fluxes at large $|z|$ to those at the interface, and in some cases undulations in ratios of perturbations of fluid variables evaluated at these two locations. It would be worthwhile to understand the origin of these undulations and how to relate their amplitudes and periods to the gravitational and MHD background parameters.

We also note that the region in the ω-k_x plane where we have seen interesting features is the "superradiant" region. It would be interesting to study in this region whether the (quadratic) time-averaged energy flux of the perturbations exhibits superradiance analogous to that for vacuum electromagnetic (and other) waves.

In our model calculations, we have used the "cold" plasma assumption [Eqs. (3.9) and (3.10)] for the model magnetosphere. This simplifies our computation but also unrealistically reduces the slow magnetosonic speed to zero. We need a more realistic equation of state to restore the slow magnetosonic critical point in our model. We have also made the idealistic assumption that the magnetic field is continuous at $z=0$, and the exiting stationary flow is ejected along $\mathbf{B}$. It should be interesting to study the effects of a "kink" in $\mathbf{B}$ to the behavior of perturbations.

Finally, we note that the study of fully dynamical "magnetospheres" in the planar spacetime (2.2) with a horizon might provide insight into the issue of whether and how a black-hole magnetosphere, if strongly perturbed, settles down into an energy-extracting, Blandford-Znajek-type[3] equilibrium state. (Punsley and Coroniti[13] argue that it does not do so.) This, of course, require a nonlinear analysis.

ACKNOWLEDGMENTS

The author is indebted to Kip Thorne, who suggested this problem and has given considerable help in the course of this work and in the writing of this manuscript. The author would like to thank Paul Coppi for help in some of the graphic presentations of the numerical results. He has also benefited from discussions with Charles Evans in dealing with numerical difficulties. This work was supported in part by NSF Grants Nos. AST85-14911 and AST88-17792.

APPENDIX

In this appendix we discuss in some detail our numerical implementation of the MHD perturbation equations [Eqs. (5.13)], and their solutions. We discuss various

checks performed on the coding process, on the numerical code and on the solutions it produces. We also identify the regions where the numerical solutions presented in Sec. VI are not reliable because of the numerical method employed.

The ODE system (5.13) is solved using the standard ODE solver, the LSODE package.[27] This package uses backward differentiation formulas (BDF) methods when the equations are stiff, which is the case for our ODE system near $z=0$, i.e., in the region where the background interacts strongly with the MHD perturbation (the process we wish to study). Thus, we used the BDF option in our code. The maximum order that we used in computing derivatives was the default value of 5. The stationary background quantities appear in coefficients of the ODE system. They were provided to the ODE solver at 402 points with uniform separations Δz in the region $-7.35 \le z \le 7.35$. The values of the ODE coefficients between these points were obtained by parabolic interpolation. The numerical solutions were output at the 402 uniformly spaced points.

At each step, the (relative) tolerance we provided to LSODE was 2×10^{-6}. However, because of the accumulation of errors and because of the internal steps used by the ODE solver in each zone, the actual global error may not be as good as this, as indicated by a test done with constant-coefficient ODE's. In this test, we construct a constant-coefficient ODE system by replacing the coefficients in Eqs. (5.13) at all other locations by their values at $z=0$. We chose the values at $z=0$ in this test because the imaginary parts of wave numbers there are the largest; i.e., the ODE system is the stiffest there and therefore this is the most difficult region for the solver to handle. We integrated the resulting ODE system starting from, in turn, only one of $\{b_z, v_x, v_z, \tilde{p}\}$ nonzero; and we then compared our numerical solutions with the analytic solutions for this constant ODE system. It was found that if we require

$$\frac{|\phi_{\text{numerical}}-\phi_{\text{analytic}}|}{(|\phi_{\text{numerical}}|+|\phi_{\text{analytic}}|)/2} \le 0.1\% \quad , \tag{A1}$$

then we can always integrate the ODE's out to $z\simeq2$ or even farther (Table I). This is such a high z that for the ODE's of our real problem, the equations have ceased to be stiff for most choices of (ω,k_x). (See Fig. 4.) However, because of (i) the stiffness of the problem at small z, near $\omega\simeq0.99k_x$, (ii) the single precision used in the numerical integration, and (iii) our lack of any way to separate globally and cleanly the growing and decaying solutions in the changing β region, the fastest decaying solutions can be completely lost to numerical truncation error even though the numerical solution and the analytic solution agree to the last digit. This loss of one solution will occur if near $z=0$, $-\mathrm{Im}(k_z)$ of the fastest decaying mode does not approach zero rapidly enough as z moves away from the interface. More specifically, if, roughly, we have, at $z=\delta L$,

$$-\mathrm{Im}(k_z)\,\delta L \sim 10 \quad , \tag{A2}$$

for the fastest decaying mode, then the single precision we used will not be adequate to preserve the decaying component of the numerical solution. As an example, in Fig. 15, we plot the local wave numbers k_z at frequency $\omega=6.5$ and wave number $k_x=6$. It is seen that $-\mathrm{Im}(k_z)$ for the fastest decaying mode is still quite significant near $z\simeq2$ truncation. This produces wild fluctuations in quantities such as $|\delta S_z(+7.35)/\delta S_z(0)|$, shown in Fig. 9(a). If we were to use double precision (and higher accuracy) in our computation, this fluctuating region would be pushed to larger k_x, i.e., to near the boundary $\omega\simeq9.99k_x$. In Fig. 16 is shown one such result computed at $\omega=6.5$, using double precision and (relative) tolerance of 2×10^{-7} at each step. Note that the fluctuation region begins only after $k_x\simeq5.5$ as opposed to $k_x\simeq4$ in Fig. 9(a), where single precision and larger tolerance 2×10^{-6} were used. This test can also serve as a global error estimate, where we use a smaller tolerance, i.e., a

TABLE I. Comparison of numerical solution and analytic solution. This is to test the implementation of the LSODE solver. The z coordinate z_0 shown in the table is the place where the two solutions begin to differ by more than 0.1%, i.e., when

$$\frac{|\phi_{\text{numerical}}-\phi_{\text{analytic}}|}{(|\phi_{\text{numerical}}|+|\phi_{\text{analytic}}|)/2} \ge 0.1\% \quad .$$

The integration starts from $z=0$, with only one of b_z, v_x, v_z, $\tilde{p}$ nonzero. This test is done for a constant matrix Q_I^J [Eq. (6.5)] with eigenvalues $k_{z,i}$: $(-0.891\,791, 1.812\,47)$, $(0.929\,320, -1.348\,87)$, $(28.8836, -0.447\,894)$, and $(29.0075, 0.992\,878)$. Here in $k_{z,i}=(a,b)$, a is the real part, b is the imaginary part.

	$b_z(z=0)\neq0$	$v_x(z=0)\neq0$	$v_z(z=0)\neq0$	$\tilde{p}(z=0)\neq0$
z_0	1.64	20.0	16.78	4.2

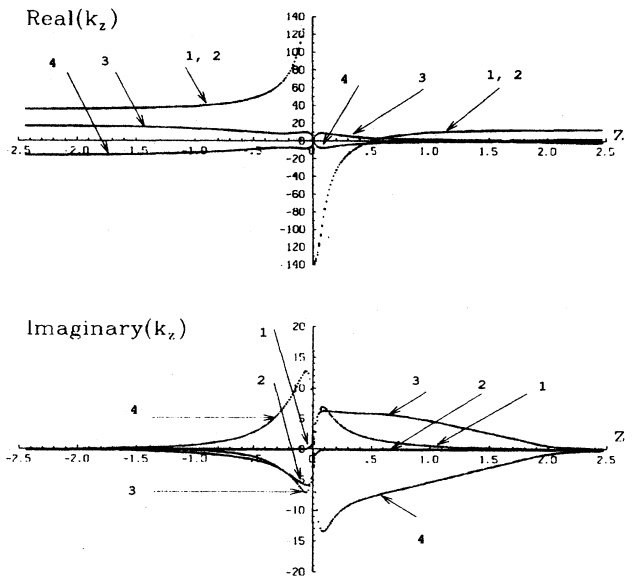

FIG. 15. Local wave numbers k_z of MHD perturbations as functions of z for the stationary background shown in Fig. 3. The perturbations have frequency $\omega=6.5$ and wave number $k_x=6$.

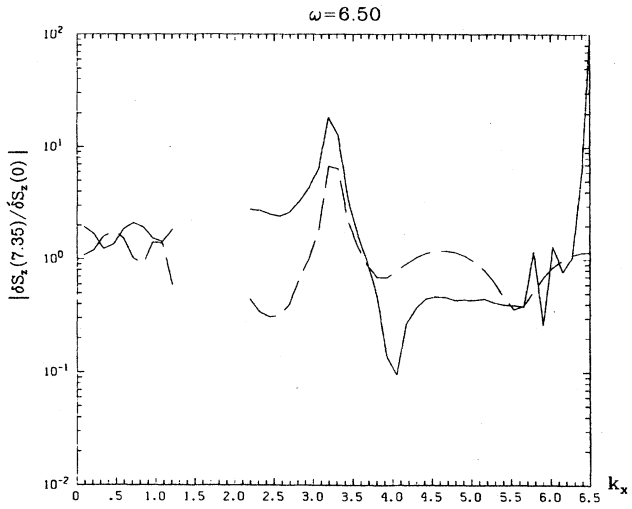

FIG. 16. The ratio $|\delta S_z(\pm 7.35)/\delta S_z(0)|$ for perturbations excited by $f_x = 10^{-6}$ alone at the interface $z=0$. The region where curves break is the region where MHD waves cannot propagate freely at $z \to -\infty$ and where numerical computations have not been done. Solid curves correspond to perturbations on the $z>0$ side; dashed curves correspond to perturbations on the $z<0$ side. This is computed with the double precision. The local tolerance used in the LSODE solver is 2×10^{-7}. Note that on the $z>0$ side, fluctuation begins at roughly $k_x \gtrsim 5.5$ as opposed to $k_x \simeq 4$ in Fig. 9, where single precision and local tolerance of 2×10^{-6} were used in that computation.

smaller step size in the integration, and the result in the nonfluctuating region stay the same.

To ensure the correct coding for our computation, we have made a few other numerical and algebraic checks: The simplest was a comparison of our numerical solutions in the uniform region (region of constant background variables) with the analytic solutions presented in Sec. V. To be more precise, one must be able to decompose the numerical solutions into individual wave modes; and each mode should evolve (with coordinate z) according to Eqs. (5.20)–(5.24). From test results shown in Table I, we know that the ODE solver as implemented will give correct numerical solutions for constant coefficient ODE's. Therefore, the key point here is that in the uniform region, our code should produce numerical solutions for each wave mode, which have the correct ratios of the amplitude of the perturbation quantities [Eqs. (5.20), (5.23), and (5.24)] and the correct dispersion relations [Eqs. (5.21) and (5.22)]. Shown in Table II are the results for such a comparison between the numerical and the analytic solutions of the magnetosonic modes for typical values of (ω, k_x). The agreement is good. They also agree quite well in tests taken at other values of (ω, k_x).

We also have to be sure that the code is implemented correctly in the nonuniform region, where the background is changing. To test the code, we have checked to see that our numerical solutions satisfy the differential energy conservation law

$$\frac{d\epsilon}{d\tau} + \nabla\cdot\delta\mathbf{S} = \beta'\delta T_{xz} \ . \tag{A3}$$

Here,

$$\epsilon = \rho\gamma u\left[\frac{1}{s}[\lambda b_x + b_z + C(Vb_z - ub_x + v_x - \lambda v_z)] + 2\gamma^3(v_x V/u + v_z) + \tilde{\rho}\gamma/u\right] , \tag{A4a}$$

$$\delta S^x = \rho\gamma u\left[2\gamma^3 V(v_x V/u + v_z) + \tilde{\rho}\gamma v/u + \gamma v_x/u + \frac{1}{s}(Vb_z - ub_x - \lambda v_z + v_x) + \frac{C}{s}b_z\right] , \tag{A4b}$$

$$\delta S_z = \rho\gamma u\left[\tilde{\rho}\gamma + 2\gamma^3(Vv_x + uv_z) + \gamma v_z/u - \frac{\lambda}{s}(Vb_z - ub_x - \lambda v_z + v_x) - \frac{C}{s}b_x\right] , \tag{A4c}$$

$$\delta T_{xz} = \rho\gamma u\left[\tilde{\rho}\gamma V + (1+2\gamma^2V^2)\gamma v_x + (1+2\gamma^2u^2)\gamma V v_z/u - \frac{1}{s}(b_x + \lambda b_z)\right] \tag{A4d}$$

are the FIDO-measured, first-order (i.e., linear in perturbation quantities) energy density, energy flux, and x-z component of stress. In Table III is shown the result of such a test. There the relative error is defined as

TABLE II. Comparison of numerical and analytic MHD wave solutions in the uniform region. Compared here are the wave numbers $k_{z,i}$ and the four components of the eigenvectors Y_i of the magnetosonic modes [see Eq. (6.6)]. This is to check the coding of MHD perturbation equations. Here complex numbers are written in the form (a,b) with a being the real part, and b the imaginary part. The two solutions are compared at $\omega=5$, $k_x=3$, and $\beta=-4$, i.e., at $z=-\infty$.

	Numerical	Analytic	Numerical	Analytic
Wave number $k_{z,i}$	−6.466 04	−6.468 32	6.344 66	6.346 91
Eigenvectors Y_i	0.626 141	0.626 08	0.902 400	0.902 377
	−0.141 465	−0.141 472	−0.076 495 2	−0.076 501 7
	−0.485 317	−0.485 341	−0.262 427	−0.262 450
	−0.593 635	−0.593 678	0.333 097	0.333 141

$$(\text{err}\%) \equiv \frac{|-i[\omega+\beta(z)k_x]\epsilon+ik_x\delta S^x+\delta S_z'-\beta'\delta T_{xz}|}{\{|[\omega+\beta(z)k_x]\epsilon|+|k_x\delta S^x|+|\delta S_z'|+|\beta'\delta T_{xz}|\}/4} .$$

In these tests, the zone size was $\Delta z=0.002$, and the largest value of the wave number was $|k_z|\lesssim 100$. Therefore, we would expect that the error should be no larger than

$$\left[\frac{1}{k_z\Delta z}\right]^2 \simeq 4\% ,$$

which is the case in these tests as shown in Table III.

Finally, as another powerful check, we have subjected the code to scrutiny by a symbolic manipulation program[28] (SMP) This check is a purely symbolic algebraic check, and the program SMP does not have any known bugs in this area. Because of the complexity of the MHD perturbation equations [Eqs. (5.13)], this check has been done in the following steps. We first coded Eq. (5.5) in the SMP format and decomposed it into its component form, consisting of terms involving MHD perturbations and their time and spatial derivatives. We also did the same for (A3). The conservation of energy (A3) is guaranteed by the equations of motion [Eq. (5.6) or (5.13)]. By expressing the time derivatives of the perturbations in terms of the perturbations themselves and their spatial derivatives, and by substituting these expressions for the time derivatives into (A3), we should have (A3) now identically zero. This is what we have done successfully using SMP. Now we have a correct form of (5.6) in the SMP format. We "translated" it into FORTRAN format to be used in our code. We also translated the resulting FORTRAN code back to SMP format and compared it with the original SMP version of the MHD equations term by term, to eliminate any possible errors in this "translation" process (one big source of errors is the correct positioning of parentheses). Our final FORTRAN code of the MHD equations was the Fourier-analyzed form of this SMP checked version, i.e., with the time derivatives in our intermediate code replaced by $-i\omega$ and derivatives with respect to x replaced by ik_x.

TABLE III. Test on numerical solutions of conservation of FIDO-measured energy. Shown in the table are relative errors at several z's. Here the relative error is defined as

$$(\text{err}\%) \equiv |-i[\omega+\beta(z)k_x]\epsilon+ik_x\delta S_x+\delta S_z' -\beta'\delta T^{xz}|/(\{|[\omega+\beta(z)k_x]\epsilon|+|k_x\delta S^x| +|\delta S_z'|+|\beta'\delta T^{xz}|\}/4) .$$

Shown in the table are results for four initial conditions starting, in turn, from one of b_z, v_x, v_z, $\tilde{\rho}$ nonzero.

	$z=0$	$z=0.4$	$z=1$	$z=3$
$b_z(z=0)\neq 0$	0.2	1.4	<0.1	0.1
$v_x(z=0)\neq 0$	0.2	1.6	0.4	0.1
$v_z(z=0)\neq 0$	0.2	0.7	0.4	<0.1
$\tilde{\rho}(z=0)\neq 0$	0.1	0.6	0.5	<0.1

To conclude, the coding of the MHD perturbation equations and their numerical solutions have been subjected to extensive checks and tests, both numerically and algebraically. These tests and checks make it very likely that there are no programming errors left. The single precision used in the computation, and the stiffness of the problem near the boundary of the integration region in the ω-k_x plane, render the solutions presented in Sec. VI not reliable in that part of the integration region. However, to show the general trend in the ω-k_x plane of various quantities, results in this unreliable region were still kept.

[1]M. J. Rees, Annu. Rev. Astron. Astrophys. **22**, 471 (1984).

[2]C. M. Gaskell and L.S. Sparke, Astrophys. J. **305**, 175 (1986); C. M. Gaskell and B.M. Peterson, Astrophys. J. Suppl. **65**, 1 (1987); J. L. Tonry, Astrophys. J. **322**, 632 (1987); A. Dressler and D. O. Richstone, *ibid.* **324**, 701 (1988); J. Kormendy, *ibid.* **325**, 128 (1988).

[3]R. O. Blandford and R. L. Znajek, Mon. Not. R. Astron. Soc. **179**, 433 (1972).

[4]Douglas Macdonald and Kip S. Thorne, Mon. Not. R. Astron. Soc. **198**, 345 (1982).

[5]E. S. Phinney, Ph.D. dissertation, University of Cambridge, 1983.

[6]P. W. Guilbert, A. C. Fabian, and M. J. Rees, Mon. Not. R. Astron. Soc. **205**, 593 (1983).

[7]M. Ruderman and P. G. Sutherland, Astrophys. J. **196**, 51 (1975).

[8]A. P. Lightman, A. A. Zdziarski, and M. J. Rees, Astrophys. J. **315**, 113 (1987).

[9]K. S. Thorne, R. H. Price, and D. A. Macdonald, *Black Holes: The Membrane Paradigm* (Yale University Press, New Haven, CT, 1986).

[10]D. A. Macdonald, Mon. Not. R. Astron. Soc. **211**, 313 (1984).

[11]C. M. Mobarry and R. V. E. Lovelace, Astrophys. J. **309**, 455 (1986).

[12]R. V. E. Lovelace, C. Mehanian, M. Mobarry, and M. E. Sulkanen, Astrophys. J. **62**, 1 (1987).

[13]B. Punsly and F. V. Coroniti, preceding paper, Phys. Rev. D **40**, 3834 (1989); UCLA Report No. PPG-1209 (unpublished).

[14]R. D. Blandford (unpublished).

[15]X.-H. Zhang, Ph.D. thesis, California Institute of Technology, 1989.

[16]S. A. Teukolsky, Phys. Rev. Lett. **29**, 1114 (1972).

[17]S. Arnowitt, S. Deser, and C. W. Misner, in *Gravitation,* edited by L. Witten (Wiley, New York, 1962), p. 227.

[18]James W. York, Jr., in *Sources of Gravitational Radiation,* edited by Larry L. Smarr (Cambridge University Press, Cambridge, England, 1979).

[19]X.-H. Zhang, Phys. Rev. D **39**, 2933 (1989).

[20]Kip S. Thorne and Douglas Macdonald, Mon. Not. R. Astron. Soc. **198**, 339 (1982).

[21]C. Michel, Astrophys. J. **157**, 1183 (1969).

[22]I. Okamoto, Mon. Not. R. Astron. Soc. **185**, 69 (1978).
[23]C. F. Kennel, F. S. Fujimura, and I. Okamoto, Geophys. Astrophys. F. Dyn. **26**, 147 (1983).
[24]T. Regge and J. A. Wheeler, Phys. Rev. **108**, 1063 (1957).
[25]J. A. Wheeler, Phys. Rev. **97**, 511 (1955).
[26]J. D. Jackson, *Classical Electrodynamics* (Wiley, New York, 1975).
[27]Alan C. Hindmarsh, in *Scientific Computing,* edited by R. S. Stepleman *et al.* (North-Holland, Amsterdam, 1983), p.55.
[28]SMP Customer Support, Inference Corp., 5300 W. Century Blvd., Los Angeles, CA 90045.
[29]I. D. Novikov and Kip S. Thorne, in *Black Holes,* edited by C. DeWitt and B. S. DeWitt (Gordon and Breach, New York, 1973), p. 343.